

---

Electronic Thesis and Dissertation Repository

---

2-23-2015 12:00 AM

## Estimating Hemodynamics in Skeletal Muscle Arteriolar Networks Reconstructed From In Vivo Data

Amani H. Saleem, *The University of Western Ontario*

Supervisor: Dr. Daniel Goldman, *The University of Western Ontario*

Joint Supervisor: Dr. Dwayne Jackson, *The University of Western Ontario*

A thesis submitted in partial fulfillment of the requirements for the Master of Science degree in Medical Biophysics

© Amani H. Saleem 2015

Follow this and additional works at: <https://ir.lib.uwo.ca/etd>



Part of the [Medical Biophysics Commons](#)

---

### Recommended Citation

Saleem, Amani H., "Estimating Hemodynamics in Skeletal Muscle Arteriolar Networks Reconstructed From In Vivo Data" (2015). *Electronic Thesis and Dissertation Repository*. 2696.  
<https://ir.lib.uwo.ca/etd/2696>

This Dissertation/Thesis is brought to you for free and open access by Scholarship@Western. It has been accepted for inclusion in Electronic Thesis and Dissertation Repository by an authorized administrator of Scholarship@Western. For more information, please contact [wlsadmin@uwo.ca](mailto:wlsadmin@uwo.ca).

ESTIMATING HEMODYNAMICS IN SKELETAL MUSCLE  
ARTERIORAL NETWORKS RECONSTRUCTED FROM IN VIVO  
DATA

(Thesis format: Integrated-Article)

by

Amani H Saleem

Graduate Program in Medical Biophysics

A thesis submitted in partial fulfillment  
of the requirements for the degree of  
Master of Science

The School of Graduate and Postdoctoral Studies  
The University of Western Ontario  
London, Ontario, Canada

© Amani H Saleem 2015

# Abstract

The objective of this work was to develop a computational model that could accurately predict blood flow in skeletal muscle arteriolar trees in the absence of complete boundary data. We used arteriolar trees in the rat gluteus maximus muscle (GM) that were reconstructed from montages obtained via intravital videomicroscopy, and incorporated a recently published method for approximating unknown boundary conditions into our existing steady-state model of two-phase blood flow. For varying numbers of unknown boundary conditions, we used the new flow model and GM arteriolar geometry to approximately match red blood cell (RBC) flows corresponding to experimental measurements. We showed that this method gives errors that decrease as the number of known boundary conditions increases. We also showed that specifying total blood flow into the arteriolar tree decreases the mean RBC flow error and its variance. By varying the target values of pressure and wall shear stress required by the model, we showed that results are less sensitive to the target pressure and, in addition, proposed a method for estimating the optimal target shear stress.

**Key words:** Mathematical Model, Skeletal Muscle, Arteriolar Tree, Intravital Videomicroscopy, Blood Flow, Fry Method, Streak Method

# Co-Authorship

A version of Chapter 2 entitled “Estimating Blood Flow in Skeletal Muscle Arteriolar Trees Reconstructed from In Vivo Data Using the Fry Approach” by Amani Saleem, Baraa Al-Khazraji, Dwayne Jackson, and Daniel Goldman is in preparation for submission to the journal *Microcirculation*. The experimental part and data collection, including network geometry reconstruction and blood flow measurements, were conducted by Baraa Al-Khazraji. Dr. Goldman and Dr. Jackson provided overall guidance of the project, and Dr. Goldman provided the initial computational blood flow code and assisted with incorporation of the Fry method. I helped developed the Fry code and performed validation, ran all simulations, and conducted analysis of the results including producing figures.



*To a great king that will always be remembered:*

*King Abdullah bin Abdulaziz, January 23, 2015*

*I cannot imagine you not being here, but I believe you will forever live on  
in the hearts of all Saudis.*

# Acknowledgments

First and foremost, I would like to thank Allah, who has given me the health, strength, and knowledge to finish this thesis successfully.

It is my pleasure to acknowledge King Abdullah bin Abdulaziz, may Allah rest his soul in peace, and the Saudi government for the opportunity to complete my education abroad, their financial support, and supervision throughout my studies via the Saudi bureau in Canada.

I would like to thank my supervisors Dr. Dwayne Jackson and Dr. Daniel Goldman for providing me with the opportunity to work in their lab. Thank you for being patient and for your useful advice and supporting throughout. This thesis would not have been completed without your guidance.

I would like to express my appreciation to all Jackson lab members for supporting me.

I especially want to thank my lovely parents Hassan and Nadia for the overwhelming amount of prayers, care, love, and encouragement I have received over the years.

I will forever be thankful to my brothers, sisters in law, nephew, and nieces for their love and kindness throughout my period of living abroad.

I would also like to thank my friend Angie for her moral support since my first day in Canada. I wish you all the best in your life.

Finally, I would like to thank my best friends and my cousins all over the world; your support and encouragement is without a doubt appreciated.

# Table of Contents

|   |            |
|---|------------|
| <b>Abstract.....</b>  | <b>ii</b>  |
| <b>Co-Authorship.....</b>   | <b>iii</b> |
| <b>Acknowledgments .....</b>                                      | <b>v</b>   |
| <b>List of Tables .....</b>                                       | <b>ix</b>  |
| <b>List of Figures.....</b>                                       | <b>x</b>   |
| <b>List of Abbreviations .....</b>                                | <b>xii</b> |
| <b>Chapter 1 .....</b>  | <b>1</b>   |
| <b>1 Introduction &amp; Background .....</b>                      | <b>1</b>   |
| <b>1.1 The Microcirculation .....</b>                             | <b>1</b>   |
| <b>1.2 Arterioles and Regulation of Flow and Resistance .....</b> | <b>3</b>   |
| <b>1.2.1 Arteriolar Regulation in Skeletal Muscle .....</b>       | <b>3</b>   |
| <b>1.3 Blood Flow in Microvessels .....</b>                       | <b>4</b>   |
| <b>1.3.1 Experimental Methods .....</b>                           | <b>5</b>   |
| <b>1.3.2 Theoretical Models.....</b>                              | <b>6</b>   |
| <b>1.4 Streak Length Method.....</b>                              | <b>7</b>   |
| <b>1.4.1 Method Description .....</b>                             | <b>8</b>   |
| <b>1.4.2 Results and Summary.....</b>                             | <b>10</b>  |
| <b>1.5 Fry Method .....</b>                                       | <b>10</b>  |
| <b>1.5.1 Approach .....</b>                                       | <b>11</b>  |
| <b>1.5.2 Results</b>  | <b>14</b>  |
| <b>1.5.3 Implications .....</b>                                   | <b>14</b>  |
| <b>1.6 Motivation and Objectives .....</b>                        | <b>18</b>  |

|  |           |
|--|-----------|
| 1.7 Thesis Outline.....  | 19        |
| 1.8 References.....  | 20        |
| Chapter 2 .....  | 26        |
| <b>2 Estimating Blood Flow in Skeletal Muscle Arteriolar Trees Reconstructed from In Vivo Data Using the Fry Approach.....</b> | <b>26</b> |
| 2.1 Introduction.....  | 26        |
| 2.2 Experimental Method.....   | 27        |
| 2.3 Computational Method .....   | 28        |
| 2.3.1 Blood flow model.....  | 28        |
| 2.3.2 Hematocrit distribution.....   | 31        |
| 2.3.3 Boundary conditions.....   | 31        |
| 2.3.4 Error measures.....  | 32        |
| 2.4 Results .....  | 33        |
| 2.4.1 Network Structure and Flow Data .....  | 33        |
| 2.4.2 Dependence of RBC Flow Error on Number and Location of Unknown Boundary Conditions .....                                 | 36        |
| 2.4.3 Sensitivity to Target Pressure and Shear Stress Values.....  | 47        |
| 2.5 Discussion .....   | 49        |
| 2.6 Conclusions.....   | 51        |
| 2.7 References.....  | 52        |
| Chapter 3 .....  | 54        |
| <b>3 Conclusions and Future Work.....</b>  | <b>54</b> |
| 3.1 Conclusions.....   | 54        |
| 3.2 Future Work.....   | 54        |
| 3.3 References.....  | 56        |

|  |           |
|--|-----------|
| <b>Appendices A: Figure Permission .....</b> | <b>57</b> |
| <b>Curriculum Vitae .....</b>                | <b>58</b> |

# List of Tables

**Table 2-1** Properties of small (SN) and large (LN) arteriolar networks reconstructed from montages of IVVM video frames. ....33

# List of Figures

|   |    |
|---|----|
| <b>Figure 1–1</b> Computer-generated map of network I. Flow directions predicted with two known boundary conditions known. Black: correct flow direction. Red: reversed flow direction. ....  | 16 |
| <b>Figure 1–2</b> Computer-generated network geometry obtained from montages of rat skeletal muscle arteriolar tree .....   | 17 |
| <b>Figure 2–1</b> Arteriolar network geometries reconstructed from IVVM. Top Row: Montages of video frames covering small network (SN, left) and large network (LN, right). Bottom Row: Skeletonized networks showing segments and nodes for SN (left) and LN (right). ....   | 34 |
| <b>Figure 2–2</b> Arteriolar vessel orderings and reference blood flow rates in small (top) and large (bottom) reconstructed networks. Orders not shown are the same as for parent vessels. ....  | 35 |
| <b>Figure 2–3</b> Blood flow vs. segment number for all known boundary conditions ('experimental flows') and single cases of unknown boundary conditions. Top: SN with unknown conditions at nodes 3A and 4A. Bottom: LN with unknown conditions at nodes 3A, 4A, 5A, and 6A .....  | 37 |
| <b>Figure 2–4</b> Blood flow rates for unknown boundary conditions vs. blood flow rates for all known boundary conditions. Top: Blood flow for SN (mean+/-SD) for 2 missing boundary conditions (10 cases). Bottom: Blood flow for LN (mean+/-SD) for 10 missing boundary conditions (100 cases). Deviation of regression lines from Y=X indicates error due to unknown boundary conditions. .... | 38 |
| <b>Figure 2–5</b> RMS RBC flow error (mean+/-SD) as a function of the number of unknown boundary conditions for SN (top) and LN (bottom). Linear regression lines show how average error increases with number of unknown boundary conditions. ....   | 40 |

**Figure 2–6** RMS RBC flow error (mean+/-SD) as a function of the number of cases considered. Results shown are for LN with  $N_{\text{unk}}=10$  and  $N_{\text{cases}}=25, 50, 100, 200$  and 400. ....41

**Figure 2–7** RMS RBC flow error (mean+/-SD) as a function of the order of unknown boundary conditions for SN (top) and LN (bottom). Linear regression line for LN shows how average error increases with arteriolar order of unknown boundary conditions.....43

**Figure 2–8** RMS RBC flow error (mean+/-SD) for LN as a function of the number of unknown boundary conditions for each arteriolar order. ....44

**Figure 2–9** Total flow error (top) and RMS RBC flow error with total flow fixed (bottom) for LN as a function of the number of unknown boundary conditions for each arteriolar order. ....45

**Figure 2–10** RMS RBC flow error (mean+/-SD) as a function of the number of unknown boundary conditions for LN with total flow fixed. ....47

**Figure 2–11** RMS RBC flow error (mean+/-SD) as a function of deviations in the target intravascular pressure  $P_0$  (top) and the target wall shear stress  $t_0$  (bottom).....48



# List of Abbreviations

|                          |                                 |
|--------------------------|---------------------------------|
| <b>RBCs</b>              | Red Blood Cells                 |
| <b>WBCs</b>              | White Blood Cells               |
| <b>Q</b>                 | Blood Flow Rate                 |
| <b>SNS</b>               | Sympathetic Nervous System      |
| <b>ESL</b>               | Endothelial Surface Layer       |
| <b>V<sub>Ratio</sub></b> | Velocity Ratio                  |
| <b>V<sub>max</sub></b>   | Maximum Red Blood Cell Velocity |
| <b>V<sub>mean</sub></b>  | Mean Blood Flow Velocity        |
| <b>IVVM</b>              | Intravital Videomicroscopy      |
| <b>GM</b>                | Gluteus Maximus Muscle          |
| <b>FITC</b>              | Fluorescein Isothiocyanate      |
| <b>SN</b>                | Small Network                   |
| <b>LN</b>                | Large Network                   |
| <b>b.c.'s</b>            | Boundary Conditions             |

## Chapter 1

### 1 Introduction & Background

Blood is a complex fluid that contains a mixture of liquid plasma, made up of water, proteins, and other dissolved substances, and particulate elements, mainly red blood cells (RBCs), white blood cells (WBCs), and platelets. In response to the pressure gradient generated by the heart, blood flows through the blood vessels of the systemic circulation to transport oxygen and carbon dioxide between the lungs and the tissues. When blood leaves the heart, it first flows into arteries, which are relatively large vessels. Arteries branch to progressively smaller vessels until reaching arterioles and then capillaries. These capillaries have very thin walls that allow oxygen to diffuse easily to nearby cells and carbon dioxide to diffuse from nearby cells into the blood. Capillaries are drained by venules that form from joining capillaries together. Smaller venules join to form progressively larger venules and eventually veins, until blood is returned from the systemic circulation to the heart by the vena cava.

As noted above, blood is a non-homogeneous fluid, but in some cases it can be treated as homogenous, in particular when studying blood flow in large arteries. However, when studying blood flow in small vessels like arterioles and capillaries we must consider blood as a suspension. This is because when vessel diameters approach the same order of magnitude as the diameter of RBCs unique rheological effects occur that substantially affect blood flow [14].

#### 1.1 The Microcirculation

The microcirculation is the part of blood circulation that consists of the smallest vessels in the body, with diameters  $\sim 100 \mu\text{m}$  or less, which are classified as arterioles, capillaries, or venules based on their anatomical location and physiological role [53]. The first major function of the microcirculation is exchange of gases (oxygen and carbon dioxide), nutrients, water, hormones, and metabolic waste products between blood and the

surrounding tissue, which means that the microcirculation is also involved in regulation of oxygen consumption and metabolism in all the body's cells [6][53].

Arterioles and venules have smooth muscle cells in their walls that control changing of their diameters (contraction or dilation) and hence blood flow (Q), since flow resistance is inversely proportional to the fourth power of diameter [53] according to Poiseuille's Law:

$$Q = \Delta P / \mathfrak{R} \quad \text{Eq.1}$$

where:

$\Delta P$  is the pressure drop

$\mathfrak{R} = 8L\eta/\pi r^4$  is the resistance

$L$  is the vessel length

$\eta$  is the blood viscosity

$r$  is the vessel radius

Arterioles are the most important vessels in controlling blood flow, since they have smaller diameters and higher resistance than venules, while venules are more important in controlling vascular volume via changes in their smooth muscle tone and diameter.

Capillaries do not have smooth muscle cells surrounding the endothelial layer and therefore cannot directly control blood flow. The main function of capillaries is exchange of O<sub>2</sub>, CO<sub>2</sub> and water between blood and the surrounding tissue. It has also been proposed that capillaries are the sites where oxygen-dependent flow regulation signals originate (via ATP release from O<sub>2</sub>-depleted RBCs), which are then conducted upstream along the capillary endothelium and cause arteriolar dilation [10][11].

It is believed that RBC perfusion of individual capillaries is regulated by passive mechanisms [8]. This means that in a given capillary bed spatial heterogeneity of RBC

flow is high under low flow conditions, but becomes lower as flow increases. Moreover, besides being spatially heterogeneous, the RBC flow within each capillary is not steady, but varies with time (temporal heterogeneity) [8].

## **1.2 Arterioles and Regulation of Flow and Resistance**

Arterioles are the smallest arteries. The inner walls of arterioles (made up mainly of endothelial cells) are surrounded by a layer of smooth muscle cells [6][53]. The smooth muscle cells are partially controlled by the sympathetic nervous system (SNS) which modulates their level of contraction according to signals from baroreceptors in the brain to increase or decrease overall vascular resistance [6]. Thus, the first major role of the arteriolar microcirculation is controlling systemic blood pressure.

The second major role of the arteriolar microcirculation is controlling local blood flow, at the level of individual tissues and tissue sub-regions, via the response of their smooth muscle cells and endothelial cells to different local factors, such as changes in shear stress, local pressure (myogenic effect), and blood oxygen level [6][14].

### **1.2.1 Arteriolar Regulation in Skeletal Muscle**

To study microcirculatory regulation, it is desirable to consider tissues that have the ability to greatly alter their blood flow and metabolism. One important tissue that has this characteristic is muscle. Muscles have three main types: skeletal muscle, heart muscle, and (vascular) smooth muscle.

Skeletal muscle makes up 40% of body mass, which means it has more microvessels than any other organ in the body. According to the microvascular structure in skeletal muscle, it is the most dynamic tissue in the body, because it has the ability to increase blood flow and metabolic rate about 20- to 50-fold, respectively [27][45]. Another main function of skeletal muscle, besides locomotion, is based on its microvascular resistance and linked to systemic blood flow and pressure regulation [29]. This a compelling reason for studying the microcirculation in skeletal muscle, because it integrates very sensitive local

regulation (to meet its own metabolic demands) and very strong global regulation (to maintain systemic blood pressure and flow).

### **1.3 Blood Flow in Microvessels**

Hemodynamics is the study of the forces involved in circulating blood through the body. The main motor behind the blood circulation is the heart, which induces arterial pressure to pump the blood. The heart is two pumps (right and left) and each pump has two chambers, the upper chambers called the atria and the lower chambers called the ventricles. There are valves between the chambers to prevent the blood from reversing direction and to enable the systemic arterial pressure to be much higher than the blood pressure in the lungs [53].

When the heart pumps the blood, there is an oscillating pressure force generated to drive blood through the vasculature. The oscillations due to the cardiac cycle are not very strong in the microcirculation, and are often not explicitly considered when studying steady-state flow in arterioles, venules and capillaries.

Measuring blood flow gives an idea of the function of the cardiovascular system and the capability of the heart and lungs to supply oxygenated blood to the tissues [53]. The microvasculature plays an important role in the transport of materials by the blood through exchange of materials (e.g.,  $O_2$ ,  $CO_2$ ) with tissues across microvessel walls [37].

Blood flow in the microcirculation differs from that in larger vessels in three main ways. First, hematocrits are variable due to the plasma skimming effect [13][32][35], which means blood volume flow and RBC flow (or discharge hematocrit) must be considered separately. Second, due to both hematocrit variability and vessel size effects, the effective blood viscosity varies in microvessels (Fahreaus-Lindqvist effect) [33][37]. This is primarily important in theoretical modeling, since it affects the pressure-flow relationship, but is also important in understanding the basic biophysics of microvascular flow. Finally, in microvessels the apparent hematocrit (volume-averaged or tube hematocrit) is lower than in larger vessels (Fahraeus effect) [37], due to the fact that RBCs travel more near the center of vessels and hence have higher average velocities

than plasma. Thus, in microvessels the tube hematocrit is typically lower than the discharge (or flow-weighted) hematocrit, which tends to be closer to the value of systemic hematocrit.

Blood flow in large vessels can be measured directly (e.g., using Doppler ultrasound [13][53], or estimated from measured values of parameters such as blood pressure and cardiac output, and values of overall tissue perfusion can also be obtained by similar methods [13]. However, these methods are not applicable to the microcirculation, and it is much more difficult to measure blood flow in individual microvessels or microvascular networks, due to the small length scales (~10 microns) and complex geometries and flow patterns usually involved [37]. For this reason, blood flow in microvessels has been studied by using a combination of experimental methods (in vivo and in vitro) and theoretical models [37].

### **1.3.1 Experimental Methods**

Measuring blood flow experimentally in microvessels means obtaining topological (connectivity), morphological (diameter and length), and hemodynamic (RBC velocity and hematocrit) information for all network vessels, although this information (particularly hemodynamics) will usually be incomplete based on in vivo studies alone [39]. Since the present work is focused on blood flow in arterioles, we focus on experimental methods for larger microvessels that typically have multiple RBCs across the lumen, rather than methods for capillaries [7][9][20][21], which typically have single-file RBC flow.

One particularly important experimental study of the microcirculation was published by Pries et al. in 1990 [39]. Data was obtained for three microvessel networks that consisted of 913, 546, and 436 vessel segments [39]. Intravital microscopy was used to scan mesenteric areas (50-80 mm<sup>2</sup>) in male Wistar rats for 40 minutes, and obtain photographs and video recordings from each field [39]. The photographs were used to get photomontages of the networks and determine diameter and vessel length at each bifurcation [39]. A microphotometric method [31][33] was used to determine tube hematocrit and discharge hematocrit values from the corresponding video recording [39].

These parameters were used as a basis for studying blood flow in microvessels by applying theoretical models, discussed in the following section.

Note that the streak length method is another, more recent technique for measuring blood flow experimentally, and will be discussed in detail in Section 1.4.

### **1.3.2 Theoretical Models**

To estimate microvascular blood flow distributions, there are many components that should be determined first, such as the vessel diameter, lengths, and topological arrangement of all segments [23][39]. If possible, each model must be validated, by comparing calculated results with experimental results [39], before being used to predict the blood flow properties of a given microvascular network.

There are several models that have been developed to simulate blood flow in microvessels based on information obtained from experimental methods. Schmid-Schönbein et al. [47] developed a model to track individual blood cells (RBCs and WBCs). Furman and Olbricht [15] worked on simulating RBC and WBC motion in a small network. Papenfuss and Gross [26] simulated blood flow in a small network (seven segments) using a continuum model, which laid the basis for most subsequent flow simulations in larger networks.

Biophysical models of blood flow in microvascular networks must consider the pressure-flow relationship in individual vessels, as well as how the RBC and plasma (and possibly other) components of blood are distributed at diverging bifurcations. The pressure-flow relationship is usually described by assuming Poiseuille's law with a variable viscosity (due to the Fahraeus-Lindqvist effect) that depends on vessel diameter and hematocrit and is obtained from experimental data. The distribution of RBCs at diverging bifurcations (plasma skimming effect) is usually described by an experimentally obtained dependence on diameters, blood flow distribution to the daughter vessels, and hematocrit of the parent vessel.

In 1990, Pries et al. [39] presented a network flow model that included empirical relations for blood viscosity (based on published human data) and plasma skimming (obtained earlier based on data in rat mesentery, Pries et al. 1989 [32]). They described an iterative procedure in which linear solutions for network blood flow (which affects hematocrit distribution) and hematocrit (which affects viscosity and hence blood flow) were alternated until steady-state values were obtained in all vessel segments. A very similar model was later published with an improved ‘in vivo’ viscosity relation [40] based on additional data in microvascular networks of the rat mesentery.

The above model [40] has been cited over 250 times and used in many studies of blood flow [13][19][36][41][46], mass transport [4][17][22] and structural changes of the microvasculature [30][34][38][42][43]. It has also been used to investigate the role of the endothelial surface layer (‘glycocalyx’) in microvascular blood flow (Pries and Secomb 2005) [35] and, in particular, to show that in vivo flow resistance can be explained by in vitro blood viscosity and the presence of an endothelial surface layer (ESL).

The models described in this section assume that all needed boundary conditions (pressure or flows at inflow and outflow vessels) are known. The Fry method [13] is an example of a blood flow model that addresses the more realistic case where not all boundary conditions are known, and will be explained in Section 1.5.

## 1.4 Streak Length Method

Recently in our laboratory, a novel experimental method was developed to measure blood flow in the skeletal muscle arteriolar tree [1]. This method can be used to obtain the profile of RBC axial velocity across the lumen, and thereby calculate the blood volume flow rate at any given location. This work also measured the velocity ratio ( $V_{\text{Ratio}}$ ), which is the maximum RBC velocity ( $V_{\text{max}}$ ) divided by the mean blood flow velocity ( $V_{\text{mean}}$ ).

Since  $V_{\text{mean}}$  times the vessel cross-sectional area gives the blood flow rate, while  $V_{\text{max}}$  (~centerline RBC velocity) is more easily measured, knowing  $V_{\text{Ratio}}$  provides a convenient means of measuring blood flow in microvessels via the equation  $Q = \pi R^2 \times V_{\text{max}} / V_{\text{Ratio}}$  where  $R$  is the lumen radius. Until the very recent development of the



‘streak length’ method (described below), most researchers used the constant value  $V_{\text{Ratio}}=1.6$  (versus 2 for Newtonian fluid) to calculate blood flow from  $V_{\text{max}}$ . This value was estimated by Baker and Wayland [2] using the dual-slit/sensor cross-correlation technique. However, it was later shown by Pittman and Ellsworth [28] that  $V_{\text{Ratio}}$  could vary substantially and depended on blood vessel diameter and the bluntness of the RBC velocity profile, as well as on the relative size of the sensor for the cross-correlation technique.

In addition, as pointed out in [1], in past studies there was a relatively small range of vessel diameters ( $\sim 17 \mu\text{m}$  to  $40 \mu\text{m}$ ) over which blood velocity was measured because of experimental and technical limitations. These past studies, in which microvascular RBC velocity profiles were obtained experimentally, considered rabbit omentum arterioles and venules [48], rabbit mesentery arterioles [25][49][50][51], and rat skeletal muscle venules [3][5].

The preceding issues motivated the study described in this section [1], in which an experimental method was developed (Streak Length Method) to provide better measurements of RBC velocity profiles in a broad range of diameters and at multiple levels of arteriolar networks. These accurate velocity profiles facilitated the process of calculating arteriolar blood flow and the RBC velocity ratio over a wider range of diameters than had previously been possible.

#### **1.4.1 Method Description**

In the streak length method, intravital videomicroscopy (IVVM) of the rat gluteus maximus muscle (GM) was used to obtain the velocity of fluorescently labeled RBCs flowing through arterioles of 6-7 week old male Sprague-Dawley rats. The arteriolar networks used provided data in 37 vessel segments with diameters ranging from  $21 \mu\text{m}$  to  $115 \mu\text{m}$ .

Streaks in IVVM images (frames) were produced by fluorescing RBCs, which were labeled with fluorescein isothiocyanate (FITC 0.4mg/mL) dye solution and injected at 1% of the animal’s total blood volume [1]. The exposure time over which these optical

images were collected was low (5 ms) for fast flow in large arterioles and higher (20 ms) for slower flow in smaller arterioles, so that ‘streaks’ could be obtained in single video frames for estimation of RBC velocities. Radial profiles of RBC velocity across the lumen were obtained from measuring the average of velocity in each lane, where lanes were obtained by dividing the cross-section of the arteriolar lumen into discrete regions approximately the width of a flowing RBC.

RBC velocities were calculated by following this equation:

$$V_{RBC} = \frac{L_{SRBC} - L_{RBC}}{T} \quad \text{Eq. 2}$$

where:

$V_{RBC}$  is RBC velocity

$L_{SRBC}$  is length of fluorescent RBC streak

$L_{RBC}$  is length of RBC

$T$  is exposure time

Since the RBC biconcave characteristic is conserved, the RBC thickness is almost constant. Additionally, RBCs have elliptical cross-section during the flow, so RBC width was set to the width of each streak. The length of the RBC along the flow direction was calculated using this equation:

$$L_{RBC} = \frac{4 A_{RBC}}{\pi W_{RBC}} \quad \text{Eq. 3}$$

where  $A_{RBC}$  is the coronal cross-sectional area for RBC, which was calculated from the average RBC diameter of  $7.18 \mu\text{m}$ , and  $W_{RBC}$  is the measured RBC width.

Using the  $V_{RBC}$  values across the lumen given by Eq. 2, the streak method integrates the velocity profile numerically (using Matlab) with the assumption that velocity is zero at the vessel wall. This gives the blood flow rate, and  $V_{\text{mean}}$  is then obtained by dividing blood flow by vessel cross-sectional area ( $A = \pi D^2/4$ ). Finally  $V_{\text{Ratio}}$  is obtained by dividing the measured  $V_{\text{max}}$  (RBC velocity on centerline) by  $V_{\text{mean}}$ :

$$V_{\text{Ratio}} = V_{\text{max}}/V_{\text{mean}} \quad \text{Eq. 4}$$

## 1.4.2 Results and Summary

Using the streak length method, arteriolar blood flow was estimated over a diameter range of 21-115  $\mu\text{m}$ , and was shown to obey a form of Murray's Law [24] with blood flow  $Q \propto D^{2.63}$  where  $D$  is the lumen diameter.  $V_{\text{Ratio}}$  was shown to vary substantially ( $\sim 1.3$  to  $2.0$ ) over this range of diameters, and the dependence of  $V_{\text{Ratio}}$  on diameter was shown to be well-approximated by the equation:

$$V_{\text{Ratio}} = 0.0071 * D + 1.15 \quad \text{Eq. 5}$$

The streak length method is an *in vivo* method that has been developed and validated successfully to quantify blood flow rates throughout the rat GM arteriolar tree, and has been used to derive a novel relationship between the velocity ratio and arteriolar diameter. While the streak length method has many other possible applications, the  $V_{\text{Ratio}}(D)$  relationship above can be used to obtain more accurate values of blood flow in arterioles independent of how  $V_{\text{max}}$  is measured.

## 1.5 Fry Method

Most previous modeling of blood flow in microvascular networks has either used a complete set of measured boundary flows [40] or (more commonly) assumed a fixed

pressure drop between the network entrance(s) and exit(s) [17]. Recently, a mathematical method was presented that can estimate blood flow distributions using incomplete information about blood flow boundary conditions [13]. The data used to develop this method were obtained from a previous experimental study with four microvascular networks [39].

### 1.5.1 Approach

This method depends on determining target values of wall shear stress and intravascular pressure from independent information about typical network hemodynamic properties, and then minimizing the squared deviations of shear stresses and pressures from these values. This minimization allows determination of pressure and flow throughout the microvascular network of interest, including at any boundary nodes where flow or pressure data were previously unknown.

The Fry method is based on the mathematical description used to solve for blood flow in a microvascular network when all boundary conditions are known. In particular, the  $M$  and  $K$  matrices described below are used.

The matrix  $M$  describes the conductance (inverse of Poiseuille resistance) of each segment and is defined as:

$$M_{jk} = \begin{cases} +\frac{\pi r_j^4}{8\mu_j \ell_j}, & \text{if } \mathbf{k} \text{ is the start node of segment } \mathbf{j} \\ -\frac{\pi r_j^4}{8\mu_j \ell_j}, & \text{if } \mathbf{k} \text{ is the end node of segment } \mathbf{j} \\ \mathbf{0}, & \text{otherwise} \end{cases} \quad \text{Eq. 6}$$

where  $r_j$  is the radius and  $\ell_j$  is the length of segment  $j$ .  $\mu_j$  is effective viscosity which is assumed to be known. Blood flow in a given segment is then

$$Q_j = \sum_{k \in N} M_{jk} P_k \quad \text{Eq. 7}$$

where  $N$  is the set of all nodes and  $P_k$  is the nodal pressure.

The  $K$  matrix describes blood flow conservation at each node and is defined as:

$$K_{ik} = \sum_{j \in S} L_{ij} M_{jk} \quad \text{Eq. 8}$$

where  $S$  denotes all segments in the network, and  $L_{ij}$  is defined as:

$$L_{ij} = \begin{cases} -1, & \text{if } i \text{ is the start node of segment } j \\ +1, & \text{if } i \text{ is the end node of segment } j \\ 0, & \text{otherwise} \end{cases} \quad \text{Eq. 9}$$

When all boundary conditions are known, the following linear problem is solved to obtain the pressures at all nodes.

$$\sum_{k \in N} K_{ik} P_k = -Q_{0i} \quad \text{for } i \in N \quad \text{Eq. 10}$$

where  $Q_{0i}$  is defined as the inflow or outflow (if negative) if  $i$  is a boundary node, and 0 otherwise.

The blood flows calculated above are used to update the hematocrit of each segment, using an equation describing the plasma skimming effect at diverging bifurcations [32] and the conservation of RBC flow at each node:

$$\sum_{j \in S} L_{ij} Q_j H_{Dj} = 0 \quad \text{for } i \in N \quad \text{Eq. 11}$$

where  $H_{Dj}$  is the discharge hematocrit in segment  $j$ , and for inflow segments Eq. 11 is replaced by specifying the inflow value of  $H_D$ .

After solving for hematocrits, the effective viscosity is recalculated using an expression for the Fahraeus-Lindqvist effect [33][37][44] and these new hematocrit values. As described in Section 1.3, the flow and hematocrit solution steps are then repeatedly alternated until convergence is reached for blood flow, hematocrit, and effective viscosity in each vessel segment and pressure at each node.

When the pressure or flows are not known at every boundary node, then a constrained minimization problem is solved such that all the equations in Eq.10 with known right-hand side (i.e., internal nodes and known boundary conditions) are satisfied.

For this method it is necessary to define target shear stresses  $\tau_{0j}$  and pressures  $P_{0k}$ . Ideally, these target values are typical for each vessel (e.g., as a function of size), but they should at least be in the physiological range to ensure that the resulting solution values are reasonable. These target values are then used to minimize the total squared deviation:

$$D = \frac{1}{2} k_p \sum_{k \in N} w_k (P_k - P_{0k})^2 + \frac{1}{2} k_\tau \sum_{j \in S} \ell_j (\tau_j - \tau_{0j})^2 \quad \text{Eq. 12}$$

where  $\tau_j$  is the wall shear stress,  $k_p$  and  $k_\tau$  are weighting factors associated with the pressure and shear deviations from the target values, and  $w_k$  is the vessel length associated with node  $k$  and defined as:

$$w_k = 1/2 \sum \ell_j \quad \text{Eq. 13}$$

where the sum is over all segments connected to node  $k$ . The wall shear stress  $\tau_j$  is defined as

$$\tau_j = c_j Q_j = c_j \sum_{k \in N} M_{jk} P_k \quad \text{Eq. 14}$$

where

$$c_j = 4\mu/\pi r_j^3 \quad \text{Eq. 15}$$

The Lagrangian objective function below is used to obtain a system of equations for all the pressures  $P_k$  in the network and the Lagrange multipliers  $\lambda_i$  are used to ensure that the fully determined equations in Eq. 10 are satisfied:

$$L = \frac{1}{2}k_p \sum_{k \in N} w_k (P_k - P_{0k})^2 + \frac{1}{2}k_\tau \sum_{j \in S} \ell_j (\tau_j - \tau_{0j})^2 + \sum_{i \in I \cup B} \lambda_i \left( \sum_{k \in N} k_{ik} P_k + Q_{0,i} \right) \quad \text{Eq. 16}$$

The governing equations are obtained by making  $L$  stationary with respect to the unknowns  $P_k$  and  $\lambda_i$ . Taking  $\partial L / \partial \lambda_i = 0$  gives the equations in Eq. 10 with known right-hand sides, while taking  $\partial L / \partial P_k = 0$  gives the remaining equations needed to solve for all the  $P_k$  and  $\lambda_i$ .

In this method there are two approaches to set the magnitudes of the target wall shear stresses  $\tau_{0j}$ . The first approach is using one fixed value for all segments, while the second approach is to calculate the target shear stress as a function of the pressure. These two approaches were shown in [13] to give very similar results.

### 1.5.2 Results

The goal of this study was to estimate blood flow distribution based on incomplete information in the microvascular network. Four microvascular networks were used with a range of segment numbers from 383 to 547 and a range of boundary nodes from 22 to 40. This method gave good results overall, when comparing the estimated results with the true values, but showed that the error increases substantially when there are a high number of unknown boundary conditions.

### 1.5.3 Implications

The Fry method was developed using microvascular networks from the mesentery (Figure 1-1), which differ both topologically and geometrically from the arteriolar networks we are considering in skeletal muscle (Figure 1-2). In particular, the mesenteric networks had multiple inlets, multiple flow paths between nodes, and relatively large vessels with diameters that did not decrease progressively from the network inflow(s) to outflows. In contrast, we are mainly interested in skeletal muscle arteriolar trees having a single inflow, unique flow paths between nodes, and a progressive increase in vessel number and decrease in vessel size as the network is traversed in the downstream direction. Therefore, it was necessary to determine if the Fry method is also applicable to these

arteriolar trees, and if so to determine the dependence of errors in flow estimation on the number of unknown boundary conditions.



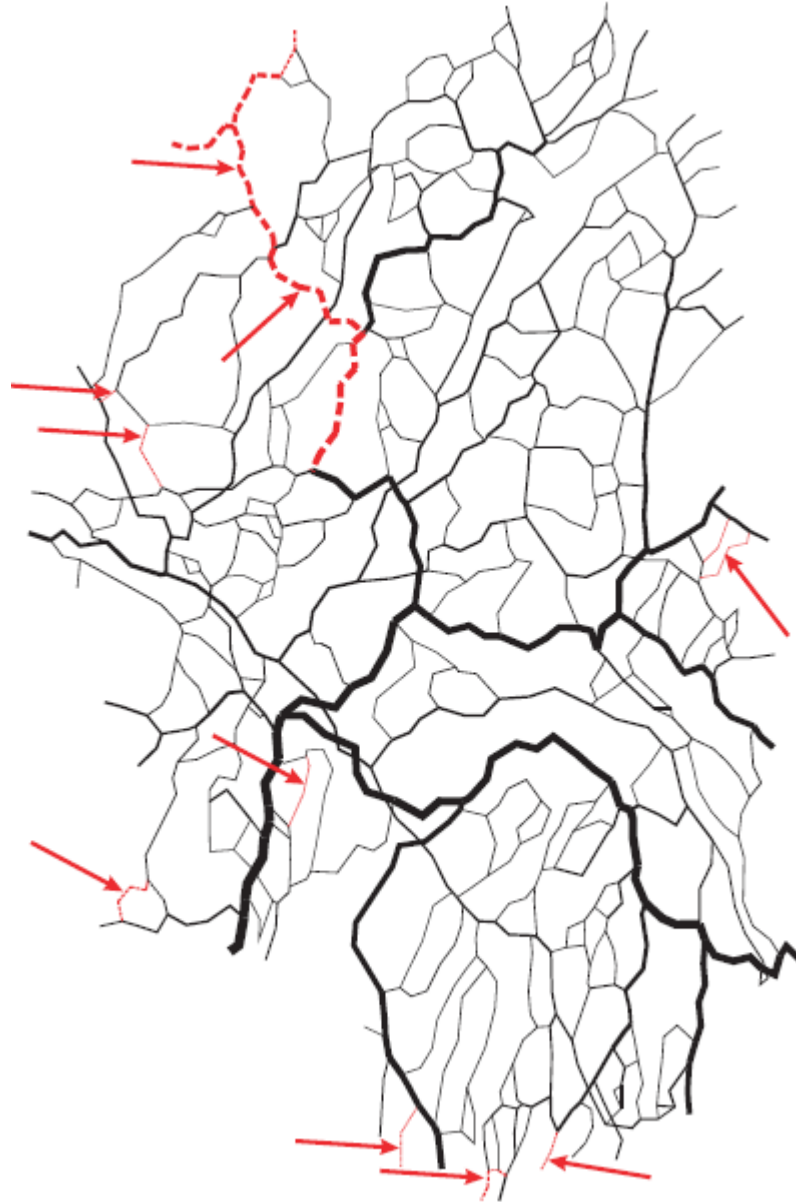


**Figure 1-1. Computer-generated map of network I in Fry et al. [13]. Flow directions predicted with two known boundary conditions known. Black: correct flow direction. Red: reversed flow direction. (Reproduced with permission, see Appendix.)**

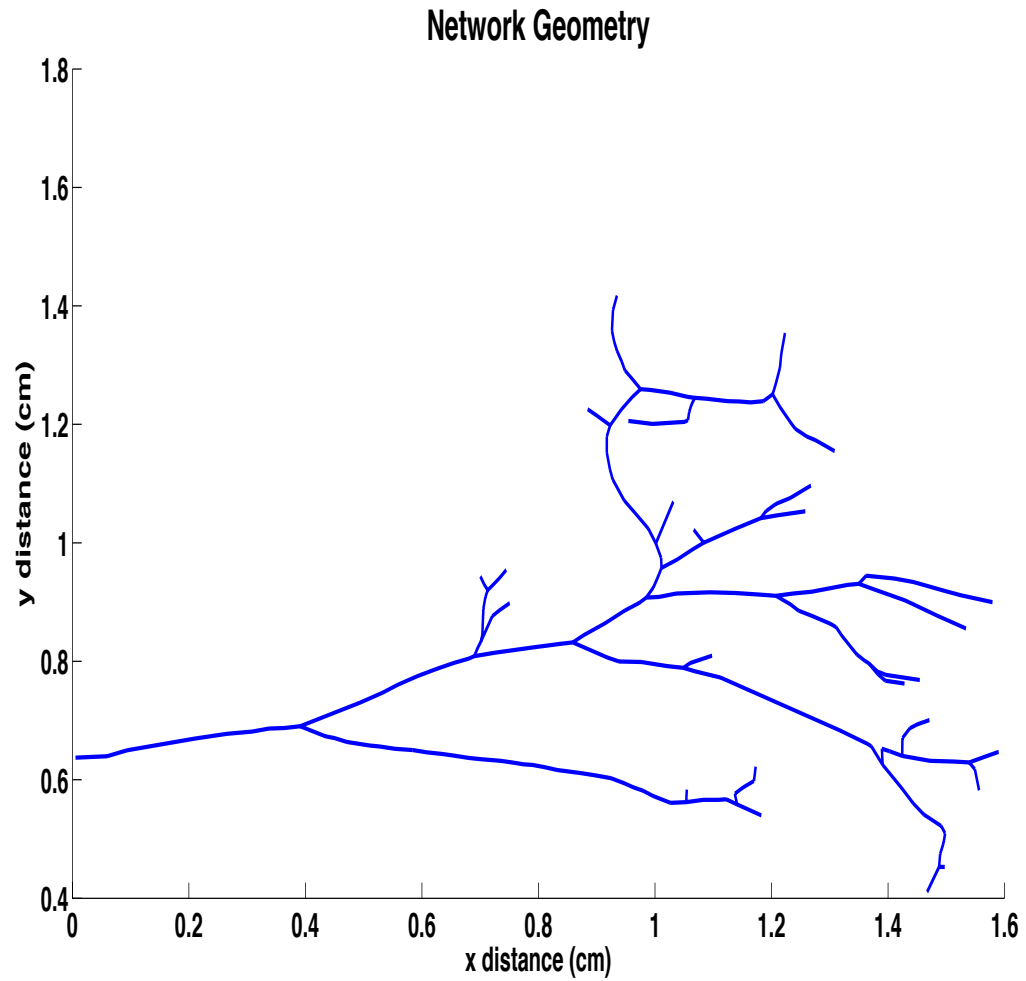


**Figure 1–2. Computer-generated network geometry obtained from montages of rat skeletal muscle (gluteus maximus) arteriolar tree in our study. Details given in Chapter 2.**

## 1.6 Motivation and Objectives

Our motivation for this project is to develop a realistic mathematical model of steady-state blood flow in skeletal muscle arteriolar trees that can be used to analyze flow resistance and predict blood flow patterns, in order to facilitate studies of microvascular flow regulation in health and in diseases such as diabetes. This method will be based on in vivo data on microvascular network structure, but needs to be robust to the absence of complete hemodynamic boundary data (obtained via the streak method). Therefore, we are developing our method based on the work of Fry described above [13] and on our group's previous work on simulating steady-state two-phase (RBCs and plasma) flow in microvascular networks [52][16][12][17][18].

The specific objectives of this project are:

- 1- To show, when some or all boundary data are unknown, that our flow model can predict blood flow patterns in skeletal muscle arteriolar trees with an error that decreases as the number of unknown boundary conditions decreases.
- 2- To determine, when some or all boundary data are unknown, if the error in predicted blood flow patterns depends on the location (in terms of arteriolar order) of the unknown boundary conditions.
- 3- To determine, when some or all boundary data are unknown, how sensitive the error in predicted blood flow patterns is to the target pressure and wall shear stress values.

## **1.7 Thesis Outline**

Chapter 2 provides an analysis of how we can apply the Fry method, which was developed by using mesenteric networks, to estimate blood flow in arteriolar trees in skeletal muscle. In particular, it addresses Objectives 1-3 described above.

Chapter 3 provides a review of important findings as well as insight into future work related to this project.

## 1.8 References

- [1] Al-Khazraji, B. K., Novielli, N. M., Goldman, D., Medeiros, P. J., & Jackson, D. N. (2012). A simple streak length method for quantifying and characterizing red blood cell velocity profiles and blood flow in rat skeletal muscle arterioles. *Microcirculation (New York, N.Y.: 1994)*, 19(4), 327-335.
- [2] Baker, M., & Wayland, H. (1974). On-line volume flow rate and velocity profile measurement for blood in microvessels. *Microvascular Research*, 7(1), 131-143.
- [3] Bishop, J. J., Nance, P. R., Popel, A. S., Intaglietta, M., & Johnson, P. C. (2004; 2003). Relationship between erythrocyte aggregate size and flow rate in skeletal muscle venules. *American Journal of Physiology - Heart and Circulatory Physiology*, 286(1), H113-120.
- [4] Chen, X., Buerk, D. G., Barbee, K. A., Kirby, P., & Jaron, D. (2011). 3D network model of NO transport in tissue. *Medical & Biological Engineering & Computing*, 49(6), 633-647.
- [5] Das, B., Bishop, J. J., Kim, S., Meiselman, H. J., Johnson, P. C., & Popel, A. S. (2007). Red blood cell velocity profiles in skeletal muscle venules at low flow rates are described by the casson model. *Clinical Hemorheology and Microcirculation*, 36(3), 217.
- [6] Den Uil, C. A., Klijin, E., Lagrand, W. K., Brugts, J. J., Ince, C., Spronk, P. E., & Simoons, M. L. (2008). The microcirculation in health and critical disease. *Progress in Cardiovascular Diseases*, 51(2), 161-170.
- [7] Ellis, C. G., Ellsworth, M. L., & Pittman, R. N. (1990). Determination of red blood cell oxygenation in vivo by dual video densitometric image analysis. *AJP - Heart and Circulatory Physiology*, 258(4), H1216.
- [8] Ellis, C. G., Wrigley, S. M., & Groom, A. C. (1994). Heterogeneity of red blood cell perfusion in capillary networks supplied by a single arteriole in resting skeletal muscle. *Circulation Research*, 75(2), 357-368.
- [9] Ellis, C. G., Ellsworth, M. L., Pittman, R. N., & Burgess, W. L. (1992). Application of image analysis for evaluation of red blood cell dynamics in

- capillaries. *Microvascular Research*, 44(2), 214-225.
- [10] Ellis, C. G., Milkovich, S., & Goldman, D. (2012). What is the efficiency of ATP signaling from erythrocytes to regulate distribution of O<sub>2</sub> supply within the microvasculature? *Microcirculation (New York, N.Y.: 1994)*, 19(5), 440.
- [11] Ellsworth, M. L., Ellis, C. G., Goldman, D., Stephenson, A. H., Dietrich, H. H., & Sprague, R. S. (2009). Erythrocytes: Oxygen sensors and modulators of vascular tone. *Physiology*, 24(2), 107-116.
- [12] Fraser, G. M., Goldman, D., & Ellis, C. G. (2012). Microvascular flow modeling using in vivo hemodynamic measurements in reconstructed 3D capillary networks. *Microcirculation (New York, N.Y.: 1994)*, 19(6), 510-520. doi:10.1111/j.1549-8719.2012.00178.x
- [13] Fry, B. C., Lee, J., Smith, N. P., & Secomb, T. W. (2012). Estimation of blood flow rates in large microvascular networks. *Microcirculation (New York, N.Y.: 1994)*, 19(6), 530-538.
- [14] Fung, Y. C. (1981). *Biomechanics: Mechanical properties of living tissues*.
- [15] Furman, M. B., & Olbricht, W. L. (1985). Unsteady cell distributions in capillary networks. *Biotechnology Progress*, 1(1), 26-32. doi:10.1002/btpr.5420010107
- [16] Goldman D., Fraser G. M., Ellis C. G., Sprague R. S., Ellsworth M. L., & Stephenson A. H. (2012). Towards a multiscale description of microvascular flow regulation: O<sub>2</sub>-dependent release of ATP from human erythrocytes and the distribution of ATP in capillary networks. *Frontiers in Physiology*, 3 doi:10.3389/fphys.2012.00246
- [17] Goldman, D., & Popel, A. S. (2000). A computational study of the effect of capillary network anastomoses and tortuosity on oxygen transport. *Journal of Theoretical Biology*, 206(2), 181-194.
- [18] Goldman D, Popel AS. Computational modeling of oxygen transport from complex capillary networks. Relation to the microcirculation physiome. *Adv Exp Med Biol*. 1999;471:555-63. PubMed PMID: 10659189.
- [19] Huang, Y., Doerschuk, C. M., & Kamm, R. D. (2001). Computational modeling of RBC and neutrophil transit through the pulmonary capillaries. *Journal of Applied Physiology*, 90(2), 545-564.

- [20] Japee, S. A. (2005). Automated method for tracking individual red blood cells within capillaries to compute velocity and oxygen saturation. *Microcirculation*, 12(6), 507-515.
- [21] Japee, S. A. (2005). A new video image analysis system to study red blood cell dynamics and oxygenation in capillary networks. *Microcirculation*, 12(6), 489-506.
- [22] Ji, J. W., Tsoukias, N. M., Goldman, D., & Popel, A. S. (2006). A computational model of oxygen transport in skeletal muscle for sprouting and splitting modes of angiogenesis. *Journal of Theoretical Biology*, 241(1), 94-108.
- [23] Lipowsky, H. H., & Zweifach, B. W. (1974). Network analysis of microcirculation of cat mesentery. *Microvascular Research*, 7(1), 73-83.
- [24] Murray, C. D. (1926). The physiological principle of minimum work. I. the vascular system and the cost of blood volume. *Proceedings of the National Academy of Sciences of the United States of America*, 12(3), 207-214. doi:10.1073/pnas.12.3.207
- [25] Nakano, A., Sugii, Y., Minamiyama, M., & Niimi, H. (2003). Measurement of red cell velocity in microvessels using particle image velocimetry (PIV). *Clinical Hemorheology and Microcirculation*, 29(3-4), 445.
- [26] Papenfuss, H., & Gross, J. (1981). Microhemodynamics of capillary networks. *Biorheology*, 18(3-6), 673-692.
- [27] Payne, G. W. (2006). The microcirculation of skeletal muscle in aging. *Microcirculation*, 13(4), 275-277.
- [28] Pittman, R. N., & Ellsworth, M. L. (1986). Estimation of red cell flow microvessels: Consequences of the baker-wayland spatial averaging model. *Microvascular Research*, 32(3), 371.
- [29] Popel, A. S., & Johnson, P. C. (2005). Microcirculation and hemorheology. *Annual Review of Fluid Mechanics*, 37(1), 43-69.
- [30] Price, R. J., Less, J. R., Van Gieson, E. J., & Skalak, T. C. (2002). Hemodynamic stresses and structural remodeling of anastomosing arteriolar networks: Design principles of collateral arterioles. *Microcirculation (New York, N.Y.: 1994)*, 9(2), 111-124.

- [31] Pries, A. R., Kanzow, G., & Gaehtgens, P. (1983). Microphotometric determination of hematocrit in small vessels. *AJP - Heart and Circulatory Physiology*, 245(1), H167.
- [32] Pries, A. R., Ley, K., Claassen, M., & Gaehtgens, P. (1989). Red cell distribution at microvascular bifurcations. *Microvascular Research*, 38(1), 81-101.
- [33] Pries, A. R., Ley, K., & Gaehtgens, P. (1986). Generalization of the fahraeus principle for microvessel networks. *AJP - Heart and Circulatory Physiology*, 251(6), H1324.
- [34] Pries, A. R., Reglin, B., & Secomb, T. W. (2001). Structural adaptation of microvascular networks: Functional roles of adaptive responses. *American Journal of Physiology - Heart and Circulatory Physiology*, 281(3), H1015-1025.
- [35] Pries, A. R., & Secomb, T. W. (2005). Microvascular blood viscosity in vivo and the endothelial surface layer. *American Journal of Physiology - Heart and Circulatory Physiology*, 289(6), H2657-2664.
- [36] Pries, A. R., Secomb, T. W., & Gaehtgens, P. (1995). Structure and hemodynamics of microvascular networks: Heterogeneity and correlations. *American Journal of Physiology*, 269(5), H1713.
- [37] Pries, A. R., Secomb, T. W., & Gaehtgens, P. (1996). Biophysical aspects of blood flow in the microvasculature. *Cardiovascular Research*, 32(4), 654-667.
- [38] Pries, A. R., Secomb, T. W., & Gaehtgens, P. (1998). Structural adaptation and stability of microvascular networks: Theory and simulations. *AJP - Heart and Circulatory Physiology*, 275(2), H349.
- [39] Pries, A. R., Secomb, T. W., Gaehtgens, P., & Gross, J. F. (1990). Blood flow in microvascular networks. experiments and simulation. *Circulation Research*, 67(4), 826-834.
- [40] Pries, A. R., Secomb, T. W., Gessner, T., Sperandio, M. B., Gross, J. F., & Gaehtgens, P. (1994). Resistance to blood flow in microvessels in vivo. *Circulation Research*, 75(5), 904-915.
- [41] Pries, A. R., Secomb, T. W., Sperandio, M., & Gaehtgens, P. (1998). Blood flow resistance during hemodilution: Effect of plasma composition. *Cardiovascular Research*, 37(1), 225-235.



- [42] Pries, A. R., Cornelissen, A. J. M., Sloot, A. A., Hinkeldey, M., Dreher, M. R., Höpfner, M., . . . Secomb, T. W. (2009). Structural adaptation and heterogeneity of normal and tumor microvascular networks. *PLoS Computational Biology*, 5(5), e1000394.
- [43] Pries, A. R., Reglin, B., & Secomb, T. W. (2005). Remodeling of blood vessels: Responses of diameter and wall thickness to hemodynamic and metabolic stimuli. *Hypertension*, 46(4), 725-731.
- [44] Pries, A. R., Secomb, T. W., & Gaehtgens, P. (1995). Design principles of vascular beds. *Circulation Research*, 77(5), 1017-1023.
- [45] Radegran, G., Blomstrand, E., Saltin, B., Institutionen för idrotts- och hälsovetenskap, Eva Blomstrands forskningsgrupp, Gymnastik- och idrottshögskolan, G., & Å...strandlaboratoriet. (1999). Peak muscle perfusion and oxygen uptake in humans: Importance of precise estimates of muscle mass. *Journal of Applied Physiology*, 87(6), 2375.
- [46] Safaeian, N., Sellier, M., & David, T. (2011). A computational model of hemodynamic parameters in cortical capillary networks. *Journal of Theoretical Biology*, 271(1), 145-156.
- [47] Schmid-Schönbein, G. W., Skalak, R., Usami, S., & Chien, S. (1980). Cell distribution in capillary networks. *Microvascular Research*, 19(1), 18-44.
- [48] Schmid-Schoenbein, G. W., & Zweifach, B. W. (1975). RBC velocity profiles in arterioles and venules of the rabbit omentum. *Microvascular Research*, 10(2), 153-164.
- [49] Tangelder, G. J., Slaaf, D. W., Arts, T., & Reneman, R. S. (1988). Wall shear rate in arterioles in vivo: Least estimates from platelet velocity profiles. *AJP - Heart and Circulatory Physiology*, 254(6), H1059.
- [50] Tangelder, G. J., Slaaf, D. W., Muijtjens, A. M., Arts, T., oude Egbrink, M. G., & Reneman, R. S. (1986). Velocity profiles of blood platelets and red blood cells flowing in arterioles of the rabbit mesentery. *Circulation Research*, 59(5), 505-514.
- [51] Tangelder, G. J., Teirlinck, H. C., Slaaf, D. W., & Reneman, R. S. (1985). Distribution of blood platelets flowing in arterioles. *AJP - Heart and Circulatory*

*Physiology*, 248(3), H318.

- [52] Tran C. H., Vigmond E. J., Goldman D., Plane F., & Welsh D. G. (2012). Electrical communication in branching arterial networks. *American Journal of Physiology - Heart and Circulatory Physiology*, 303(6), 680-692. doi:10.1152/ajpheart.00261.2012
- [53] Waite, L., & Fine, J. M. (2007). Applied biofluid mechanics.

## Chapter 2

# 2 Estimating Blood Flow in Skeletal Muscle Arteriolar Trees Reconstructed from In Vivo Data Using the Fry Approach

## 2.1 Introduction

Skeletal muscle makes up approximately 40% of human body mass, and besides being necessary for locomotion its dense arteriolar networks contribute greatly to total peripheral resistance, a key component of blood pressure regulation [5][6]. Skeletal muscle has the capacity to greatly increase its blood flow rate and rate of aerobic metabolism (about 20- to 50-fold, respectively) [3][5][13]. Branching arteriolar networks in skeletal muscle are also able to control distribution of blood flow to terminal arterioles and capillary networks and to the specific groups of muscle fibers they supply [6]. On the other hand, given its large volume of vasculature and its ability to greatly alter resistance, skeletal muscle is strongly innervated by the sympathetic nervous system (SNS) to maintain/increase vascular tone in inactive muscles and organs, which serves to maintain/increase blood pressure. This mechanism buffers steep decreases in blood pressure in the face of orthostatic/exercise stress while increasing blood flow to active muscle and vital organs [1].

Our group has been focused on studying SNS control of arteriolar diameter and blood flow in rat skeletal muscle using intravital videomicroscopy (IVVM). In particular, we have been studying the action of various SNS receptor types at different levels in the arteriolar tree under a range of conditions, including diabetes [3][4]. We have recently developed a novel rat gluteus maximus (GM) preparation that allows observation of complete arteriolar trees, from first-order feed arterioles down to fifth- and sixth-order arterioles which supply the terminal arterioles [1]. We have also developed a novel streak-length method [1] that uses fluorescently labeled red blood cells (RBCs) to measure RBC velocities and blood flow rates over large portions of the GM arteriolar tree. However, it is difficult and time-consuming to apply the streak-length method to

entire arteriolar trees. This makes it desirable to have a computational model that can approximate any missing flow data, and also integrate available flow data to enforce mass conservation and address any measurement errors or fluctuations during the time it takes to capture data over a complete tree. Although methods have been developed for selecting vessels in which to measure flow in microvascular networks [14], these methods do not give estimates of missing flows or boundary data, or the error caused by missing boundary conditions.

Steady-state two-phase (RBCs and plasma) models of blood flow in microvascular networks have existed for some time [11][12], but they generally require complete data on the boundaries of the network (inflow and outflow segments). However, since in our work on arteriolar trees in the GM some of the missing flow data are on the boundaries, we needed a blood flow model that does not require complete boundary data. Such a method was recently published by Fry et al [2] and validated using microvascular geometry and blood flow data from IVVM experiments on the rat mesentery. Since mesentery microvasculature has completely different geometry, topology, and regulation compared to arteriolar trees in skeletal muscle, it was the objective of the present work to apply the Fry approach to arteriolar trees in the rat GM to determine how well it would perform. We also wanted to find methods that would optimize the performance of a Fry-type blood flow model given the GM arteriolar geometry and the types of flow data we expect to be available in our ongoing IVVM experiments.

## **2.2 Experimental Method**

The experimental data used in this study was obtained from previous *in vivo* experiments performed in our laboratory on the rat gluteus maximus (GM) muscle. The animal preparation and intravital videomicroscopy (IVVM) techniques used are described in detail in [1]. Also described in [1] is the ‘streak length method’ used to obtain RBC velocity measurements and estimates of blood flow within arteriolar trees in the GM under steady-state resting (i.e., control) conditions.

Multiple fields of view acquired to obtain blood flow data were aligned manually using Photoshop into montages, which allowed for reconstruction of continuous portions of the arteriolar tree. Lengths, diameters and connectivities of arterioles, from a single first order vessel (1A) down through several levels of bifurcations, were obtained via measurements made on montages using Matlab. These data were then assembled into network data files that could be input into our blood flow simulation codes.

For the present work, two reconstructed networks were used. The small network (SN) consisted of 9 arteriolar vessels. For this network, experimental measurements of blood flow were obtained in all vessels including those on the boundaries (inflow and outflow vessels). To ensure compatibility with our blood flow model, adjustments were made manually so that blood flow was conserved at all nodes joining two or three vessels.

The large network (LN) consisted of 49 arteriolar vessels. For this network, experimental measurements of blood flow were not obtained in all vessels, but flows throughout the network were estimated manually to maintain consistency with the flow-diameter relationship established in [1]. Our blood flow model (described below) was then applied (with manual adjustment of boundary pressures) to ensure that blood flow was conserved at all nodes.

To evaluate the importance of the location within the network of unknown boundary conditions, we determined the order of vessels (1A-6A) in SN and LN using centrifugal ordering, with an increase in vessel order being induced by a daughter-to-parent branch angle greater than 18 degrees or a daughter-to-parent diameter ratio less than 0.8.

## **2.3 Computational Method**

### **2.3.1 Blood flow model**

The two-phase (RBCs and plasma) continuum blood flow model used in this study consisted of two component models that were solved alternately until a steady-state solution was reached for all variables. The first model described the intravascular

pressures and blood volume flow rates throughout the arteriolar network, assuming fixed viscosity in each vascular segment.

Our blood flow model utilized the approach of Fry et al. [2] to solve for blood flow both when all boundary conditions (flows or pressures at all inflow and outflow vessels) are known and when some boundary conditions are unknown. For clarity, we reproduce below the key equations originally presented in [2].

When all boundary conditions are known, the following linear system of equations is solved:

$$\sum_{k \in N} K_{ik} P_k = -Q_{0i} \text{ for } i \in N \quad \text{Eq. 17}$$

where  $N$  is the set of nodes,  $P_k$  is the pressure at node  $k$ ,  $Q_{0i}$  are known blood flow rates at boundary nodes and zero for internal nodes, and  $K_{ik} = \sum_{j \in S} L_{ij} M_{jk}$  where  $S$  is the set of vessel segments. The conductivity matrix  $M_{jk}$  is given by

$$M_{jk} = \begin{cases} +\frac{\pi r_j^4}{8\mu_j \ell_j}, & \text{if } \mathbf{k} \text{ is the start node of segment } \mathbf{j} \\ -\frac{\pi r_j^4}{8\mu_j \ell_j}, & \text{if } \mathbf{k} \text{ is the end node of segment } \mathbf{j} \\ \mathbf{0}, & \text{otherwise} \end{cases} \quad \text{Eq. 18}$$

where  $r_j$  is the radius of segment  $j$ ,  $\ell_j$  is the length of segment  $j$ , and  $\mu_j$  is the local blood viscosity in segment  $j$ . Finally, mass conservation is described by the matrix  $L_{ij}$ :

$$L_{ij} = \begin{cases} -1, & \text{if } i \text{ is the start node of segment } j \\ +1, & \text{if } i \text{ is the end node of segment } j \\ 0, & \text{otherwise} \end{cases} \quad \text{Eq. 19}$$

(Note that in Eq. 17 a pressure condition can be applied at boundary node  $i$  by setting  $K_{ii}=1$  and  $K_{ij}=0$  for  $j \neq i$ , and replacing  $Q_{0i}$  by  $-P_{0i}$ .)

When some boundary conditions are unknown, Eq. 17 cannot be solved for boundary nodes with unknown conditions. In this case, target values for the wall shear stresses  $\tau_{0j}$  and the intravascular pressures  $P_{0k}$  are used to obtain an error minimization problem that results in a linear system of equations at all the nodes. In particular, the error to be minimized is defined as

$$D = \frac{1}{2} k_p \sum_{k \in N} w_k (P_k - P_{0k})^2 + \frac{1}{2} k_\tau \sum_{j \in S} \ell_j (\tau_j - \tau_{0j})^2 \quad \text{Eq. 20}$$

where  $\tau_j$  is the wall shear stress,  $k_p$  and  $k_\tau$  are weighting factors associated with the deviations from the target pressures and shear stresses, respectively, and  $w_k$  is the vessel length associated with node  $k$ , which is defined as  $w_k = 1/2 \sum \ell_j$  where the sum is over all segments connected to node  $k$ . The wall shear stress  $\tau_j$  is defined as

$$\tau_j = c_j Q_j = c_j \sum_{k \in N} M_{jk} P_k \quad \text{Eq. 21}$$

where  $c_j = 4\mu_j/\pi r_j^3$ .

Including the constraint that Eq.17 is satisfied at all nodes that are internal or have known boundary values leads to the additional equations

$$k_\tau \sum_{k \in N} H_{ik} P_k + k_p w_i (P_i - P_0) + \sum_{k \in I \cup B} K_{ki} \lambda_k = k_\tau \sum_{j \in S} \tau_{0j} c_j M_{ji} \ell_j \quad \text{for } i \in N \quad \text{Eq. 22}$$

where  $I$  and  $B$  are the sets of internal nodes and boundary nodes with known conditions, respectively,  $\lambda_k$  are the Lagrange multipliers, and  $H_{ik} = \sum_{j \in S} c_j^2 M_{ji} M_{jk} \ell_j$ .

The number of pressures  $P_i$  to be determined equals the number of elements in  $N$ , which is the size of the linear system given by Eq. 22. The number of Lagrange multipliers  $\lambda_k$  to be determined equals the number of elements in  $I \cup B$ , which is the size of the fully

determined system given by Eq. 17. Therefore, solving these two equations simultaneously yields all the required  $P_i$  and  $\lambda_k$ .

It was shown in [2] that similar results are obtained for the following two approaches: i. assuming  $\tau_{0j}$  is a function of segment pressure  $P_j$  (mean of pressure at two end nodes) based on previous experimental data and ii. assuming  $\tau_{0j}$  has a single fixed value  $\tau_0$ . We have used the second approach, taking a single shear stress target value  $\tau_0$  for each network considered, since it is simpler and does not require a known relation between segment pressure and wall shear stress. For SN we used  $\tau_0= 18.41$  dyne/cm<sup>2</sup> and  $P_0= 76.38$  mmHg, while for LN we used  $\tau_0= 27.24$  dyne/cm<sup>2</sup> and  $P_0= 40.05$  mmHg, with all target values given by the mean values when all boundary conditions were known. For both networks, we used  $k_\tau= 0.4$  and  $k_p= 0.1$  based on the results in Fry et al. [13].

### **2.3.2 Hematocrit distribution**

The second model used in our calculation of two-phase blood flow determined the hematocrit distribution and hence the effective viscosity throughout the arteriolar network. To calculate the hematocrit distribution, blood flow values from the flow model are used to enforce conservation of RBC flow at each node. In addition, an empirical bifurcation rule [7][9] is used at diverging bifurcations to determine RBC flow distributions to the two daughter branches as a function of the blood flow distribution at the bifurcation, the daughter diameters, and the hematocrit in the parent vessel. Solution of the resulting linear system of equations yields discharge hematocrit values throughout the network, which allow calculation of the local blood viscosities based on an empirical description of the Fahraeus-Lindqvist effect [8][10]. Blood flows are then re-calculated using these new viscosity values, and the flow and hematocrit solution steps are repeated until all pressures, blood flows and hematocrits converge to constant values [2].

### **2.3.3 Boundary conditions**

To solve for the blood flow rates in a given network, a pressure value must be set for at least one of the boundary nodes, since it is only pressure differences that are determined by the blood flow model equations. In our flow simulations we set the pressure at the



inflow node, and then consider flow conditions for the remaining boundary values. Although both pressure and flow cannot be set at the inflow node in the above framework, we consider cases where total flow into the network is also fixed by specifying flow in one of the internal segments in the first-order arteriole. To solve for the hematocrits in a given network, hematocrit must be set at all the inflow segments. In our flow simulations, we set the discharge hematocrit in the single inflow segment (first segment of first-order arteriole) to 0.42.

### 2.3.4 Error measures

To compare RBC flow distributions obtained with one or more unknown boundary conditions to those obtained with all known boundary conditions (assumed to represent the exact experimental RBC flow distribution), the root mean square RBC flow error across all segments in the network (SN or LN) was computed:

$$RFE_{rms} = \sqrt{\frac{1}{N} \sum_{i=1}^N (Q_i^{all} H_{Di}^{all} - Q_i^{Nunk} H_{Di}^{Nunk})^2} \quad \text{Eq. 23}$$

where  $N$  is the number of segments in the network of interest,  $Q_i^{all}$  and  $H_{Di}^{all}$  are the flows and discharge hematocrits (respectively) in the network with all known boundary conditions, and  $Q_i^{Nunk}$  and  $H_{Di}^{Nunk}$  are the flows and discharge hematocrits (respectively) in the network with a given set of  $N_{unk} \geq 1$  unknown boundary conditions. The relative RMS RBC flow error is defined as  $RFE_{rms}^{rel} = RFE_{rms}/RF_{rms}$  where

$$RF_{rms} = \sqrt{\frac{1}{N} \sum_{i=1}^N (Q_i^{all} H_{Di}^{all})^2} \quad \text{Eq. 24}$$

We also use the error in total blood flow to the network,  $TFE = |Q_1^{all} - Q_1^{Nunk}|$ , where  $i=1$  is the inflow segment to the network of interest. When more than one case (i.e., set) of missing boundary conditions is considered for a given network and value of  $N_{unk}$ , the mean error (either  $RFE_{rms}^{rel}$  or  $TFE$ ) over all cases simulated is considered.

## 2.4 Results

### 2.4.1 Network Structure and Flow Data

Parameters for the reconstructed small (SN) and large (LN) arteriolar networks are given in Table 2-1, and the networks are shown in Figures 2-1. In Figure 2-1, the two top panels show montages of IVVM video frames used to obtain arteriolar geometry. The bottom panels contain the skeletonized forms showing node locations, segment lengths and vessel connectivities obtained from these montages. Figure 2-2 shows segment diameters and the blood flow distributions that were taken to represent experimental flow data, as well as the centrifugal ordering of each vessel. The complete boundary data (pressures and/or flows) needed to obtain these flow distributions using our hemodynamic model are considered to be the correct (known) boundary conditions. In addition, the RBC flow distributions obtained by applying our flow model to these networks with all known boundary conditions are taken to be the experimental values.

**Table 2-1. Properties of small (SN) and large (LN) arteriolar networks reconstructed from montages of IVVM video frames.**

| Net-work | Order Range | Segments | Total Length (cm) | Diameter Range ( $\mu\text{m}$ ) | Boundary Segments |    |    |    |    | Total Flow (ml/s)    |
|----------|-------------|----------|-------------------|----------------------------------|-------------------|----|----|----|----|----------------------|
|          |             |          |                   |                                  | 2A                | 3A | 4A | 5A | 6A |                      |
| SN       | 1A-4A       | 37       | 1.02              | 36-95                            | 1                 | 3  | 1  | 0  | 0  | $4.93 \cdot 10^{-5}$ |
| LN       | 1A-6A       | 222      | 6.41              | 10-125                           | 0                 | 6  | 9  | 7  | 3  | $5.34 \cdot 10^{-5}$ |

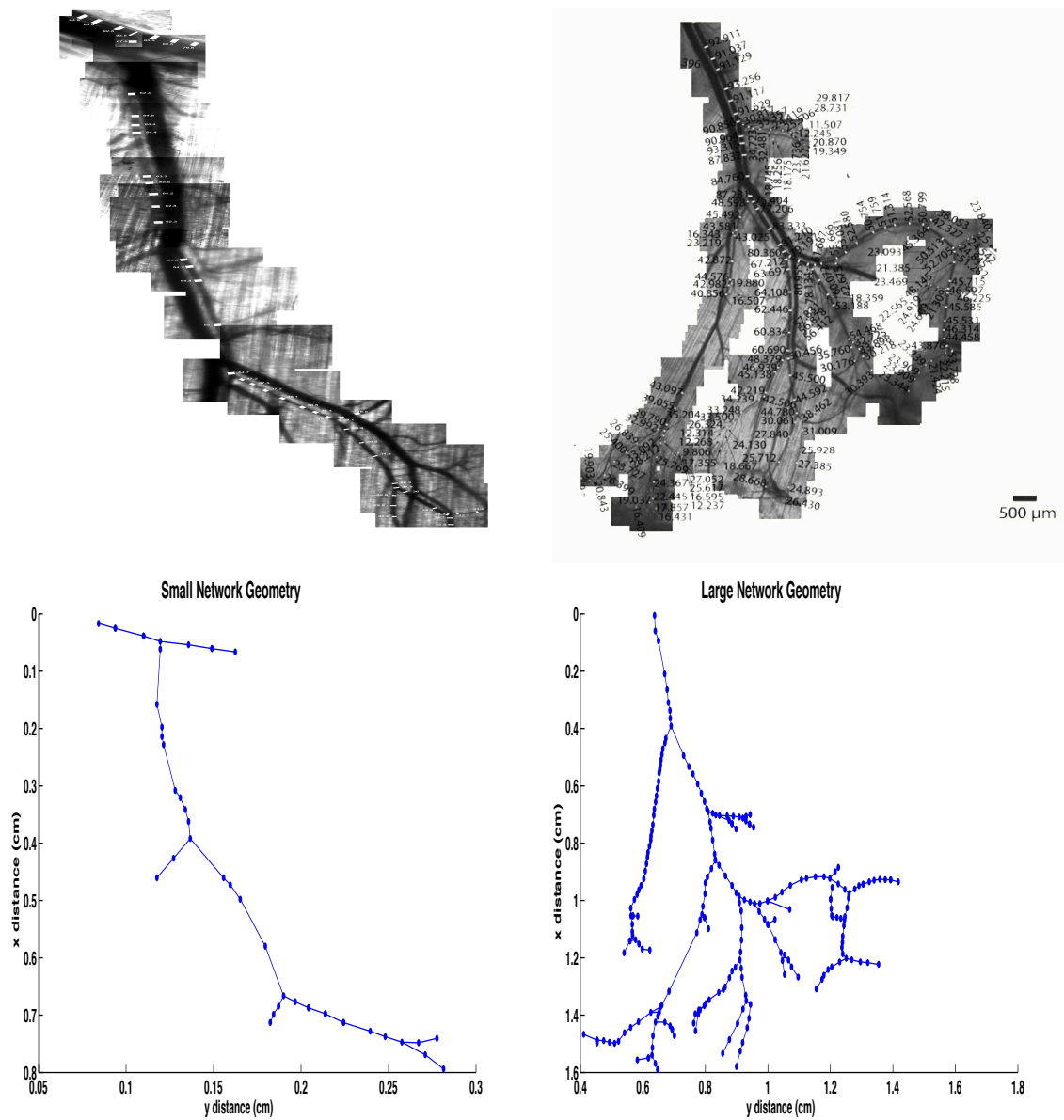


**Figure 2–1. Arteriolar network geometries reconstructed from IVVM. Top Row: Montages of video frames covering small network (SN, left) and large network (LN, right). Bottom Row: Skeletonized networks showing segments and nodes for SN (left) and LN (right).**

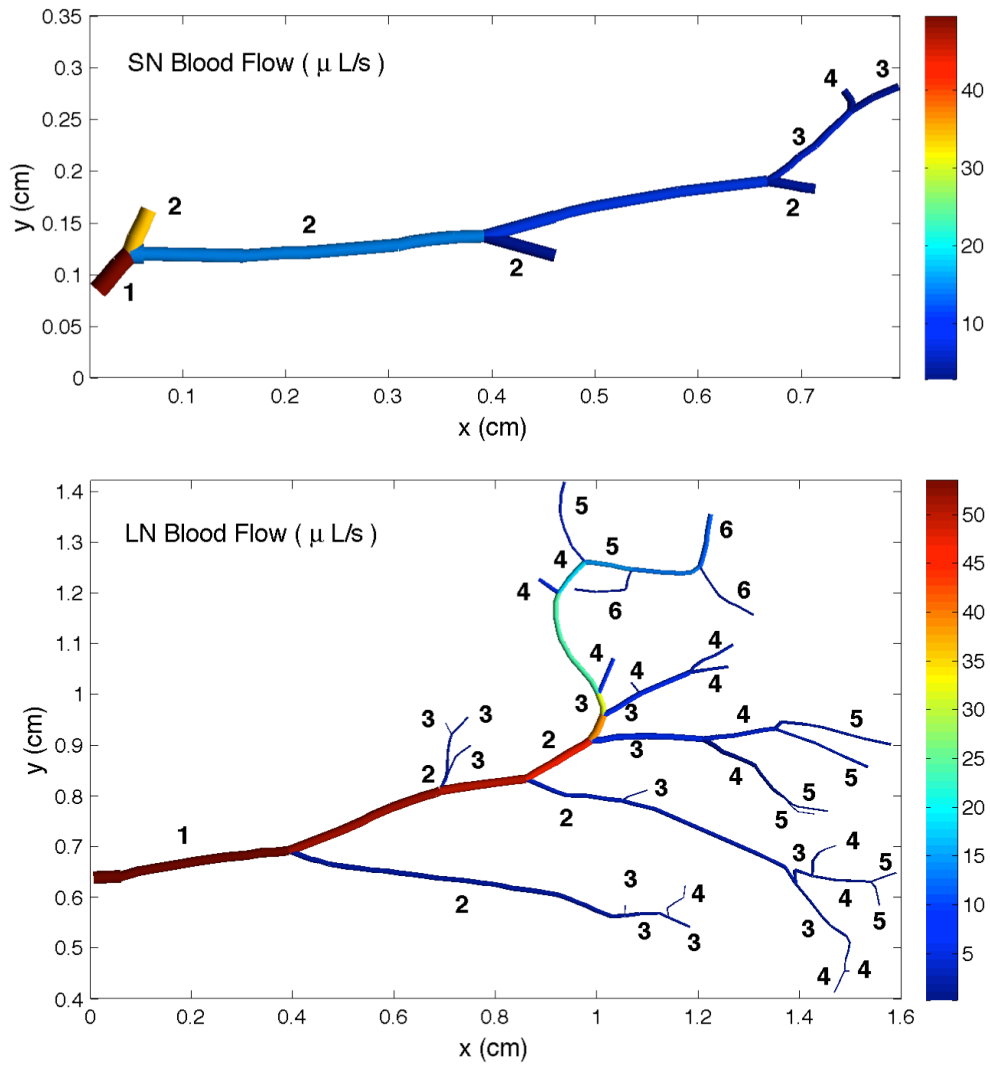


**Figure 2–2. Arteriolar vessel orderings and reference blood flow rates in small (SN, top) and large (LN, bottom) reconstructed networks. Orders not shown are the same as for parent vessels.**

### **2.4.2 Dependence of RBC Flow Error on Number and Location of Unknown Boundary Conditions**

To determine how well our flow method would perform when not all boundary conditions are known, we simulated blood flows in SN and LN for increasing numbers of unspecified boundary conditions. As described above, fixed values for  $\tau_0$  and  $P_0$  were used for each network, based on the mean values obtained for the flow solutions when all boundary conditions were specified. In all cases for SN and LN the inlet pressure was specified (80 mmHg for SN, 50.5 mmHg for LN), meaning the maximum number of unknown boundary conditions was one less than the total number of boundary nodes (5 and 25 for SN and LN, respectively). Figure 2-3 shows the deviation from the experimental flow distributions for two cases of solutions obtained with unknown boundary conditions. Figure 2-4 compares the average blood flow rates obtained for SN and LN with 2 and 10 unknown boundary conditions, respectively, to the corresponding blood flow rates for all known boundary conditions.

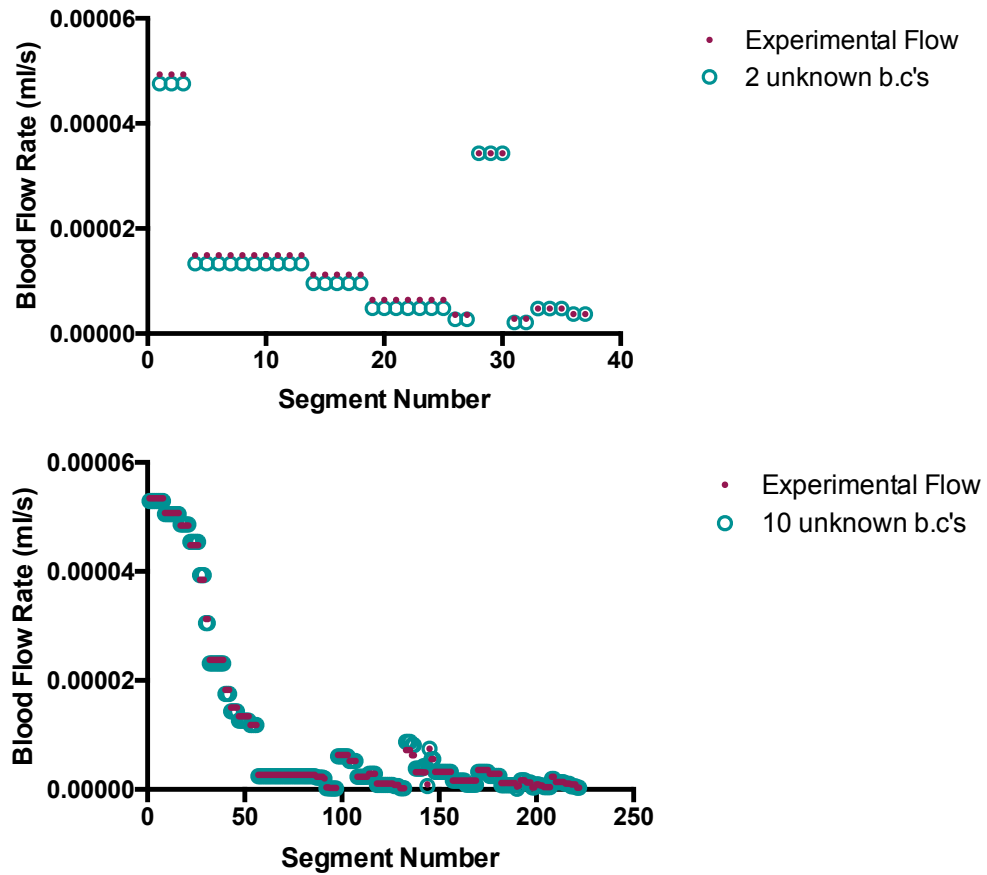


Figure 2–3. Blood flow vs. segment number for all known boundary conditions ('experimental flows') and single cases of unknown boundary conditions. Top: SN with unknown conditions in segments 27 and 32. Bottom: LN with unknown conditions in segments 93, 97, 129, 141, 143, 144, 169, 190, 217, and 220.

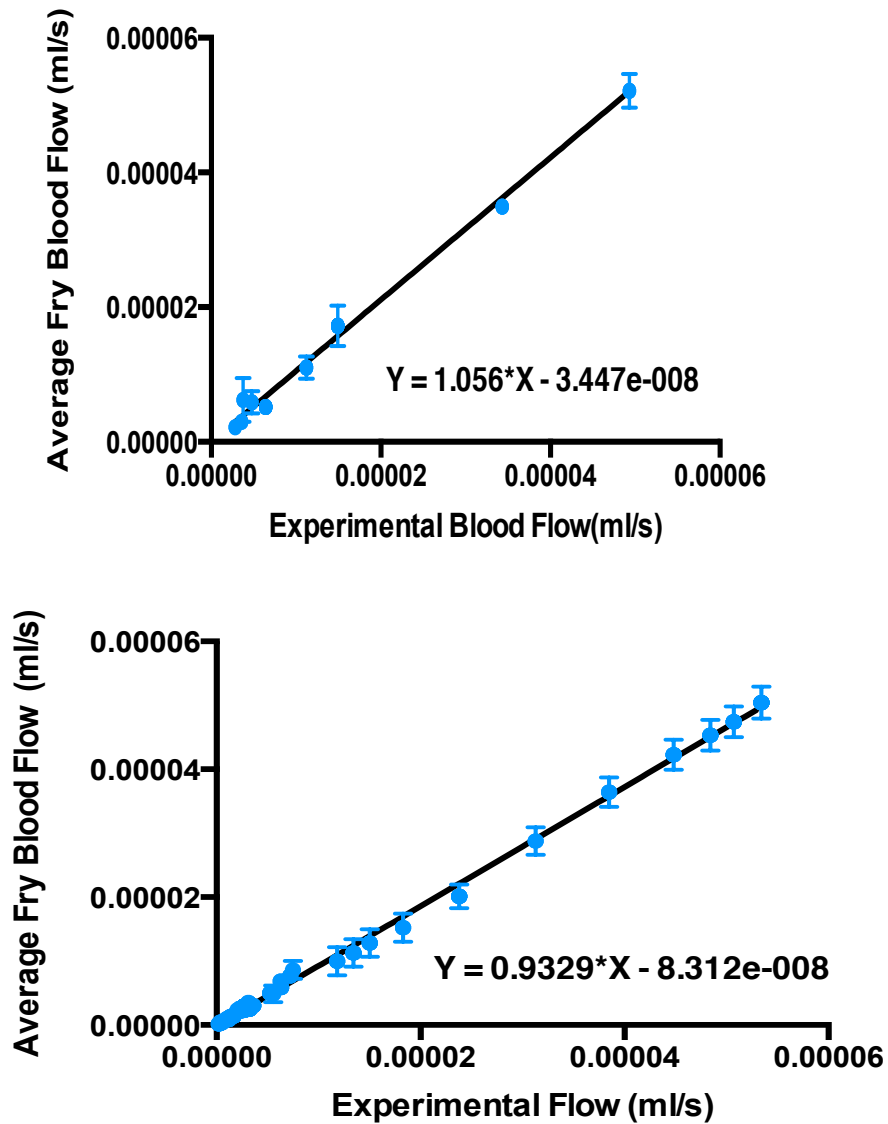


Figure 2–4. Blood flow rates for unknown boundary conditions vs. blood flow rates for all known boundary conditions. Top: Blood flow for SN (mean+/-SD) for 2 missing boundary conditions (10 cases). Bottom: Blood flow for LN (mean+/-SD) for 10 missing boundary conditions (100 cases). Deviation of regression lines from  $Y=X$  indicates error due to unknown boundary conditions.

Figure 2-5 shows how  $RFE_{rms}^{rel}$  increases as the number of unknown boundary conditions increases. For SN, all possible combinations of unknown boundary conditions were simulated, since the number of combinations ( $N_{cases}$ ) varied between 1 (for  $N_{unk}=5$  unknown boundary conditions) and 10 (for  $N_{unk}=2$  and 3). For LN,  $N_{cases}$  quickly becomes intractably large (e.g.,  $N_{unk}=5$  gives  $N_{cases}=[25 \text{ choose } 5]=53130$ ), so the number of cases considered for each value of  $N_{unk}$  was set to a maximum of 100. This meant that for LN all possible combinations were only simulated for  $N_{unk}=1$ . For both SN and LN,  $RFE_{rms}^{rel}$  decreased as  $N_{unk}$  decreased. Although the standard deviations in Figure 2-5 are large, the trends are clear and showed statistical significance in both networks ( $p=0.0014$  and  $p=0.0001$  for SN and LN, respectively).



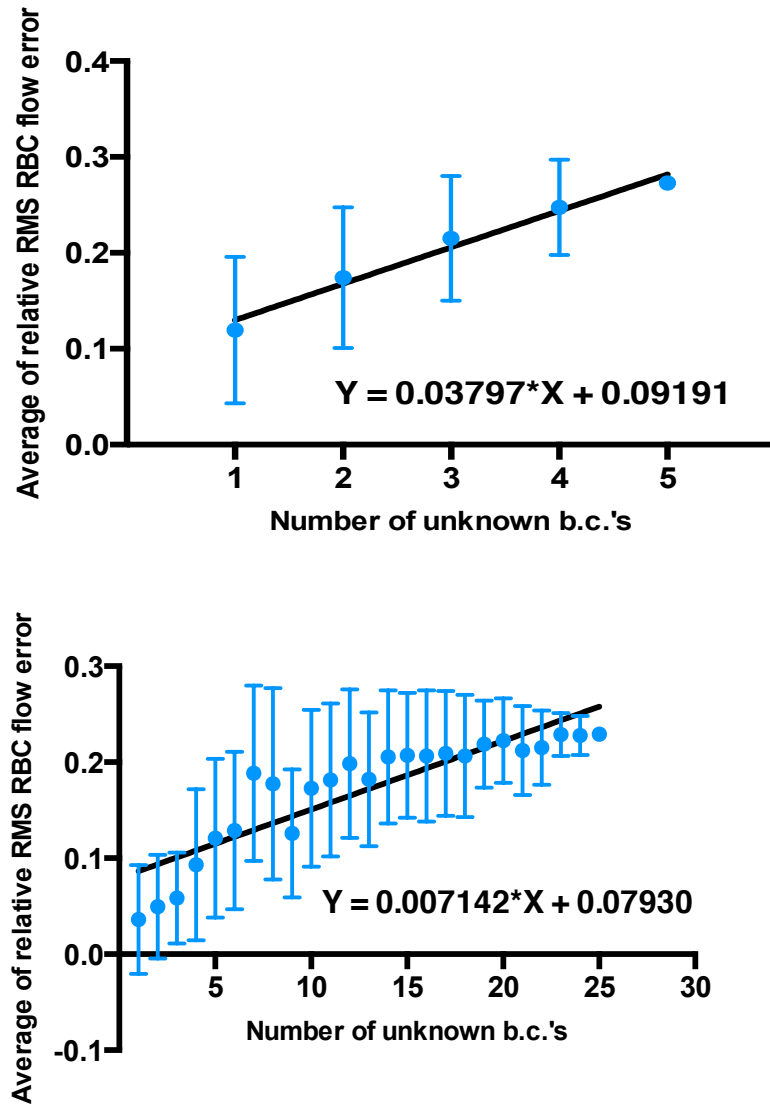


Figure 2–5. RMS RBC flow error (mean $\pm$ SD) as a function of the number of unknown boundary conditions for SN (top) and LN (bottom). Linear regression lines show how average error increases with number of unknown boundary conditions.

To test the effect of taking  $N_{\text{cases}} \leq 100$  with LN, for  $N_{\text{unk}}=10$  we looked at  $RFE_{rms}^{rel}$  and its standard deviation  $std(RFE_{rms}^{rel})$  for  $N_{\text{cases}}=25, 50, 100, 200,$  and  $400$ . As seen in Figure 2-6, there were only minor changes in  $RFE_{rms}^{rel}$  and  $std(RFE_{rms}^{rel})$  for  $N_{\text{cases}} \geq 50$ .

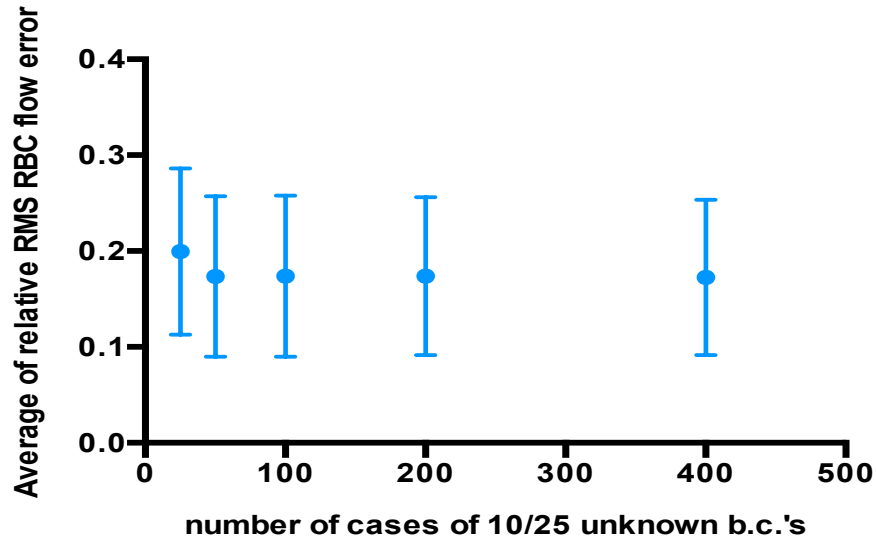


Figure 2–6. RMS RBC flow error (mean+/-SD) as a function of the number of cases considered. Results shown are for LN with  $N_{\text{unk}}=10$  and  $N_{\text{cases}}=25, 50, 100, 200$  and  $400$ .

To determine whether the flow estimation error depends on the location of unknown boundary conditions, we separated boundary conditions according to the centrifugal order of the vessels involved. Figure 2-7 shows how  $RFE_{rms}^{rel}$  changes as a function of order, where for each order all possible values of  $N_{unk}$  (from 1 to number of boundary conditions for that order) and all possible cases for each  $N_{unk}$  were considered and the errors averaged. In addition, the highest two orders in each network were combined to represent all the most distal vessels in the reconstructed network. For SN there was no significant change in  $RFE_{rms}^{rel}$  with order ( $p=0.38$ ), but for LN there was an increase with increasing order including orders 5 and 6 combined ( $p=0.03$ ).

To further investigate the dependence of  $RFE_{rms}^{rel}$  on the order of the vessels with unknown boundary data, we considered  $RFE_{rms}^{rel}$  as a function of  $N_{unk}$  within each order for LN. These results, shown in Figure 2-8, indicate that  $RFE_{rms}^{rel}$  does not increase substantially with  $N_{unk}$  for 1A-5A, but does for 6A and 6A combined with 5A.

Since 6A vessels are the most distal in LN, we examined whether total flow changed more when 6A boundary data was unknown. The results for TFE as a function of  $N_{unk}$  within each order, shown in top panel of Figure 2-9, confirm this. We therefore recalculated  $RFE_{rms}^{rel}$  as a function of  $N_{unk}$  within orders 5A, 6A, and 5A+6A with total flow to the network fixed. These results, presented in the bottom panel of Figure 2-9, show that  $RFE_{rms}^{rel}$  is greatly reduced and becomes comparable to (or slightly smaller than) the values found for unknown boundary conditions of orders 3-5 (c.f. Figure 2-8), for which TFE increased only slightly with  $N_{unk}$ .

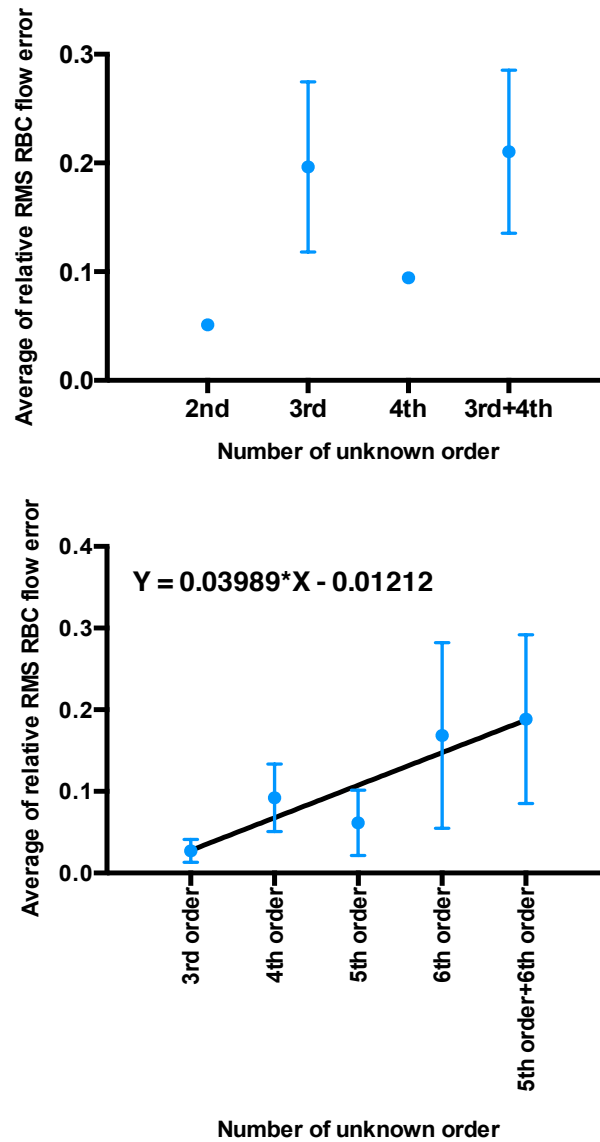


Figure 2-7. RMS RBC flow error (mean+/-SD) as a function of the order of unknown boundary conditions for SN (top) and LN (bottom). Linear regression line for LN shows how average error increases with arteriolar order of unknown boundary conditions.

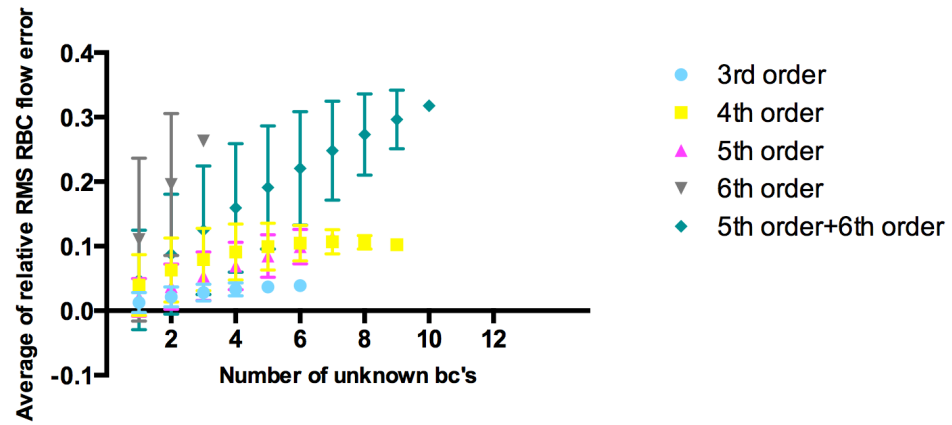


Figure 2–8. RMS RBC flow error (mean+/-SD) for LN as a function of the number of unknown boundary conditions for each arteriolar order.

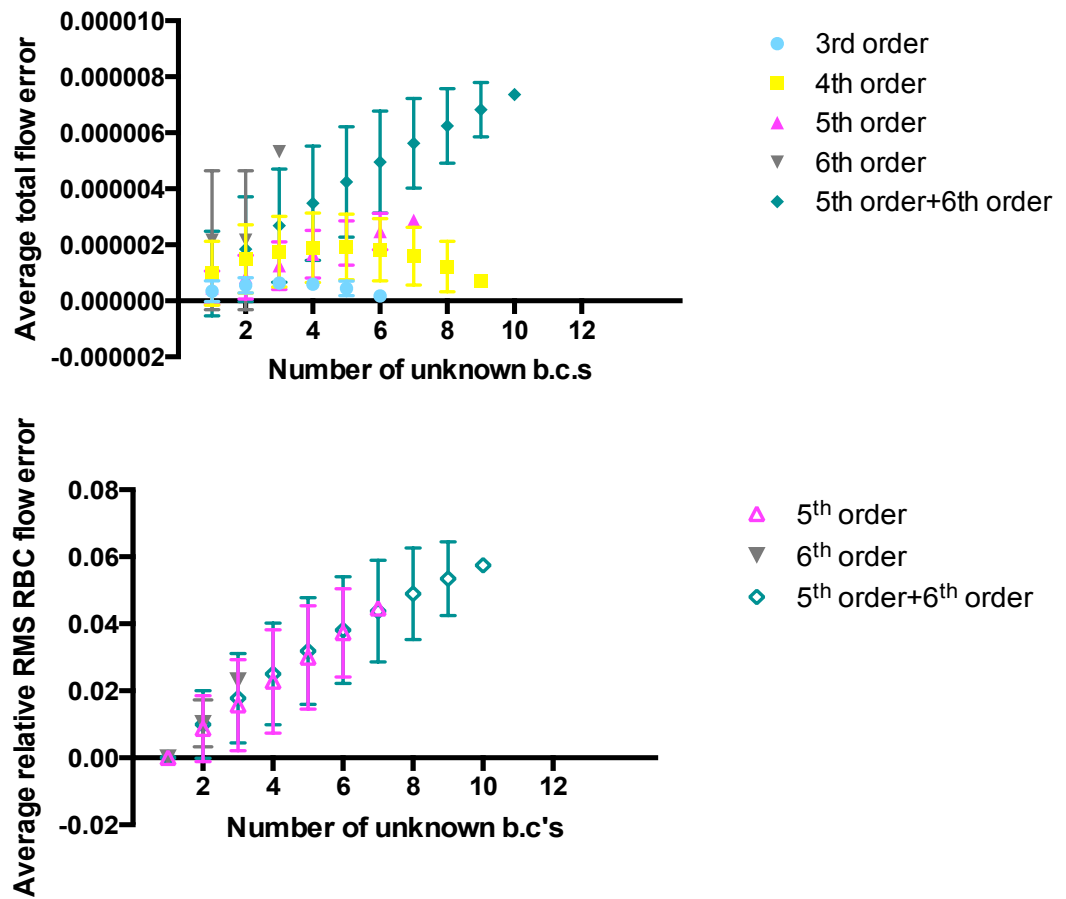


Figure 2-9. Total flow error in ml/s (top) and RMS RBC flow error with total flow fixed (bottom) for LN as a function of the number of unknown boundary conditions for each arteriolar order.

Given the above results for  $RFE_{rms}^{rel}$  with unknown 5<sup>th</sup> and/or 6<sup>th</sup> order boundary conditions when total flow is fixed, we compute  $RFE_{rms}^{rel}$  for the full range of possible unknown boundary conditions (100 cases per  $N_{unk}$ ). These results, shown in Figure 2-10, demonstrate that knowing total flow substantially decreases  $RFE_{rms}^{rel}$  as well as its standard deviation (c.f. Figure 2-5).

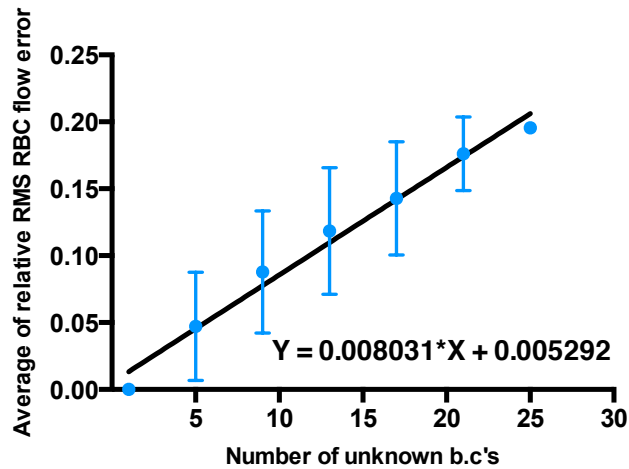


Figure 2–10. RMS RBC flow error (mean $\pm$ SD) as a function of the number of unknown boundary conditions for LN with total flow fixed.

### 2.4.3 Sensitivity to Target Pressure and Shear Stress Values

In the results presented above, the values of  $P_0$  and  $\tau_0$  were estimated from knowledge of the correct flow distributions in SN and LN. However, normally this would not be the case in a network to which we are applying our Fry-based blood flow model. To examine the effect of errors in  $P_0$  and  $\tau_0$  on estimated blood flow distributions, we vary  $P_0$  and  $\tau_0$  by  $\pm 50\%$  for the case of 10 missing boundary conditions in LN. These results, presented in Figure 2-11, show that  $RF E_{rms}^{rel}$  is more sensitive to  $\tau_0$  than to  $P_0$  (note different vertical scales in the two plots). These results also show that the actual value of  $P_0$  used was higher than the optimal value, while the value of  $\tau_0$  used was slightly lower than the optimal value.



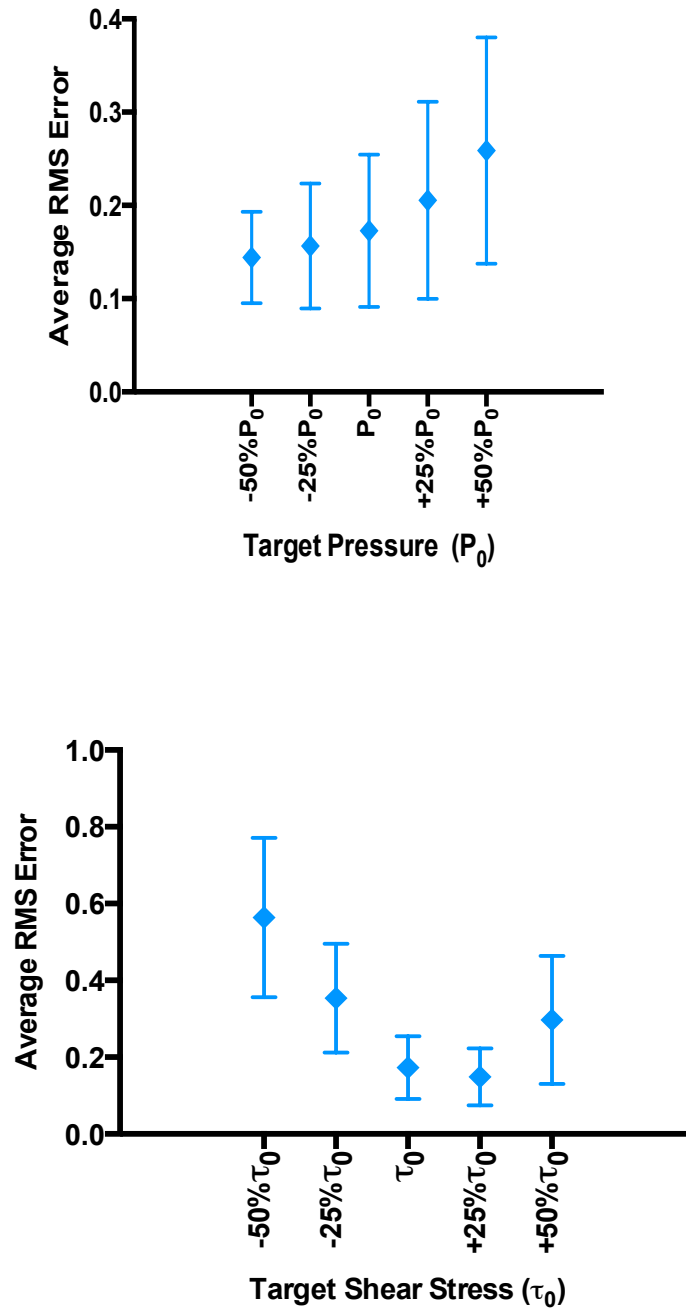


Figure 2–11. RMS RBC flow error (mean $\pm$ SD) as a function of deviations in the target intravascular pressure  $P_0$  (top) and the target wall shear stress  $\tau_0$  (bottom).

## 2.5 Discussion

Using data from the mesentery, Fry et al. [2] developed a method for estimating blood flow in microvascular networks when some boundary conditions are unknown. We have shown that the Fry approach can also be applied to arteriolar trees in skeletal muscle. In particular, we have shown (Figure 2-5) that the average relative RBC flow error in a given network decreases as the number of unknown boundary conditions decreases.

The preceding average results were quite promising; however, the variability of the error (as measured by standard deviation) was quite large, an issue which was not addressed in [2]. This suggested that either most boundary conditions must be known (e.g., 20/25) to reliably approximate network blood flow, or boundary conditions at specific key locations (or arteriolar orders) in the network must be known.

Using centrifugal ordering of the arterioles in the small network (SN) and the large network (LN), we showed that the average RBC flow error does not depend strongly on the order of the vessels where boundary conditions are unknown (Figure 2-7), except when the vessels are the most distal ones (i.e., 6A) in a large arteriolar tree (Figure 2-8). However, boundary data on the highest order arterioles in a network (with diameters of  $\sim 10\text{-}15\ \mu\text{m}$ ) is challenging to obtain, and these vessels are generally more numerous (e.g., if 5A and 6A are combined) than lower order vessels.

To address the above issue, we considered the error in estimated total blood flow to LN, and found that it was related to missing 6A boundary data (Figure 2-9). In particular, we found that if total blood flow was specified (which would require data in a single 1A vessel or small number of 2A vessels), then average RBC flow error due to missing 6A (or 5A and 6A) boundary data was significantly reduced. This effect can be seen by comparing the results in Figure 2-8 to the lower panel in Figure 2-9.

As can be seen by comparing Figure 2-10 to the lower panel of Figure 2-5, setting total blood flow in LN leads to a more rapid decrease in the average RBC flow error as the number of unknown boundary conditions decreases (without considering orders). It also leads to a more consistent decrease in the error, and this holds even when standard

deviations are considered. For  $N_{\text{unk}}=10$  (the total number of 5A and 6A boundary conditions in LN), setting total flow gives an average error of  $\sim 0.085$  with a standard deviation of  $\sim 0.050$ , compared to an average error of  $\sim 0.150$  with a standard deviation of  $\sim 0.100$  when total flow is unspecified. Similarly, for  $N_{\text{unk}}=19$  (the total number of 4A, 5A and 6A boundary nodes), setting total flow gives an average error of  $\sim 0.158$  with a standard deviation of  $\sim 0.040$ , compared to an average error of  $\sim 0.215$  with a standard deviation of  $\sim 0.050$  when total flow is unspecified. Thus, in the situation where enough data are available to estimate total flow directly, the Fry approach yields estimates of the RBC flow distribution within the network that increase in accuracy with the amount of additional boundary flow data available.

An important practical issue we tried to address was selecting target values for the wall shear stress  $\tau_0$  and pressure  $P_0$  as required in the Fry method. Our results (Figure 2-11) suggest that the RBC flow error is less sensitive to  $P_0$  than to  $\tau_0$ . They also show that lower values of  $P_0$  give better results, which suggests that  $P_0$  should reflect typical outflow pressures rather than averages over the entire network. In contrast to our results for  $P_0$ , our results for the dependence of the RBC flow error on  $\tau_0$  show that the target shear stress should be close to the average wall shear stress over the entire network. We have not explored how this value for  $\tau_0$  might be found for a given network, but since average shear stress and total network flow should be proportional to each other, it might be possible to vary  $\tau_0$  without fixing total flow until the measured value of total flow is obtained.

Although we believe the results presented are reliable, they do have two limitations that need to be discussed. First, blood flow was not measured throughout LN and therefore what we have considered as the exact flow distribution is only an approximation. However, this approximation was developed independent of the present work, based on the flow and diameter relationship established in [1], and did not consider target shear stress or pressure values as in the Fry approach. A similar approach to estimating missing network flow data for the purpose of testing a hemodynamic model was used by Pries et al. [11]. In addition, SN, for which we did have complete measured flow data, was also used in our study. As can be seen in Figure 2-5, SN showed a similar decrease in RBC

flow error with increasing number of known boundary conditions, which supports the results using LN. Second, although it should be possible to measure hematocrit using the streak method, the methodology for doing so has not yet been developed, and therefore hematocrit data were not available for either SN or LN. Despite this, we felt that RBC flow was a better (and possibly more sensitive) quantity to use for measuring the error than blood flow, considering that: i. the empirical relation describing RBC distribution at diverging bifurcations [7][9] is well established and ii. hematocrit needed to be calculated in order to estimate local viscosity and blood flow distributions.

## **2.6 Conclusions**

We have shown that the Fry method [2] can be used for estimating blood flow in arteriolar trees in skeletal muscle when the boundary data are incomplete, and that the average RBC flow error decreases as the number of known boundary conditions increases. We have also shown that setting total blood flow in such microvascular networks increases the rate at which the average RBC flow error decreases with increasing number of known boundary conditions, and also decreases the variability in the error. Since measuring the total flow in an arteriolar tree is usually possible during IVVM experiments (using the streak method), the approach described here can be applied to actual experiments and should yield more complete results on hemodynamics in large arteriolar trees (particularly in the numerous higher order arterioles) than was previously possible.

## 2.7 References

- [1] Al-Khazraji, B. K., Novielli, N. M., Goldman, D., Medeiros, P. J., & Jackson, D. N. (2012). A simple “Streak length method” for quantifying and characterizing red blood cell velocity profiles and blood flow in rat skeletal muscle arterioles. *Microcirculation*, *19*(4), 327-335. doi:10.1111/j.1549-8719.2012.00165.x
- [2] Fry, B. C., Lee, J., Smith, N. P., & Secomb, T. W. (2012). Estimation of blood flow rates in large microvascular networks. *Microcirculation*, *19*(6), 530-538. doi:10.1111/j.1549-8719.2012.00184.x
- [3] Novielli, N. M., & Jackson, D. N. (2014). Contraction-evoked vasodilation and functional hyperaemia are compromised in branching skeletal muscle arterioles of young pre-diabetic mice. *Acta Physiologica*, *211*(2), 371-384. doi:10.1111/apha.12297
- [4] Novielli, N. M., Al-Khazraji, B. K., Medeiros, P. J., Goldman, D., & Jackson, D. N. (2012). Pre-diabetes augments neuropeptide Y1- and  $\alpha$ 1-receptor control of basal hindlimb vascular tone in young ZDF rats. *PLoS One*, *7*(10), e46659. doi:10.1371/journal.pone.0046659
- [5] Payne, G. W. (2006). The microcirculation of skeletal muscle in aging. *Microcirculation*, *13*(4), 275-277.
- [6] Popel, A. S., & Johnson, P. C. (2005). Microcirculation and hemorheology. *Annual Review of Fluid Mechanics*, *37*(1), 43-69.
- [7] Pries, A. R., Ley, K., Claassen, M., & Gaehtgens, P. (1989). Red cell distribution at microvascular bifurcations. *Microvascular Research*, *38*(1), 81-101.
- [8] Pries, A. R., Ley, K., & Gaehtgens, P. (1986). Generalization of the fahraeus principle for microvessel networks. *AJP - Heart and Circulatory Physiology*, *251*(6), H1324.
- [9] Pries, A. R., & Secomb, T. W. (2005). Microvascular blood viscosity in vivo and the endothelial surface layer. *American Journal of Physiology - Heart and Circulatory Physiology*, *289*(6), H2657-2664.
- [10] Pries, A. R., Secomb, T. W., & Gaehtgens, P. (1996). Biophysical aspects of blood flow in the microvasculature. *Cardiovascular Research*, *32*(4), 654-667.

- [11] Pries, A. R., Secomb, T. W., Gaehtgens, P., & Gross, J. F. (1990). Blood flow in microvascular networks. experiments and simulation. *Circulation Research*, 67(4), 826-834.
- [12] Pries, A. R., Secomb, T. W., Gessner, T., Sperandio, M. B., Gross, J. F., & Gaehtgens, P. (1994). Resistance to blood flow in microvessels in vivo. *Circulation Research*, 75(5), 904-915.
- [13] Radegran, G., Blomstrand, E., Saltin, B., Institutionen för idrotts- och hälsovetenskap, Eva Blomstrands forskningsgrupp, Gymnastik- och idrottshögskolan, G., & Å...strandlaboratoriet. (1999). Peak muscle perfusion and oxygen uptake in humans: Importance of precise estimates of muscle mass. *Journal of Applied Physiology*, 87(6), 2375.
- [14] Wetter, T., Hoffmann, D., & Schmid-Schönbein, H. (1983). Analysis of network flow distribution: Computational aid to minimize experimental expenditure. *Microvascular Research*, 26(2), 221-237.

## Chapter 3

### 3 Conclusions and Future Work

#### 3.1 Conclusions

As demonstrated by the results in Chapter 2, we have accomplished most of the objectives of this study. In particular, we have shown that our flow model can predict RBC flow distribution in skeletal muscle arteriolar trees with an error that decreases as the number of unknown boundary conditions decreases. We extended the results obtained by Fry et al. [1] in mesentery networks to arteriolar trees in skeletal muscle, and calculated the mean and variance of the RBC flow error for a large number of cases which was not done in [1]. We have also shown that for large arteriolar trees (i.e., LN) the RBC flow distribution is most sensitive to missing boundary conditions in 5<sup>th</sup> and especially 6<sup>th</sup> order arterioles. We demonstrated that this sensitivity was related to the total flow error, and showed how it could be overcome by specifying total blood flow. Finally, we have calculated the dependence of the results on the target pressure  $P_0$  and target shear stress  $\tau_0$ , and found the dependence on  $P_0$  for arteriolar trees was somewhat different from that in mesentery (where higher rather than lower  $P_0$  gave better results). The RBC flow error was shown to be more sensitive to  $\tau_0$  than to  $P_0$ , and we therefore proposed a practical method for estimating  $\tau_0$  based on total flow. Thus, we have developed and validated a method for estimating blood flow in arteriolar trees of skeletal muscle that can be applied to data on geometry and blood flow being obtained in the IVVM experiments on skeletal muscle in our own laboratory and in similar microvascular research laboratories elsewhere.

#### 3.2 Future Work

Although the present results are a significant advance in estimating arteriolar hemodynamics in skeletal muscle, there are several types of future studies that are needed. It would be an important confirmation of the present results to apply our flow estimation method to a large network (such as LN) with full blood flow data for all vessels in the network. It would also be worthwhile to apply our method to a network in

which both volume flow and hematocrit had been measured. A future direction would be applying our method in an arteriolar tree to which a vasoconstrictor or vasodilator has been applied. In this case, it should still be possible to estimate  $P_0$  and  $\tau_0$  (given data on total flow), and the method should then give similar accuracy to that found in the present work. However, the accuracy of our method would again need to be shown by comparison to full network blood flow data. Similarly, the performance of our method could be tested in a disease state (such as diabetes) to determine whether changes in flow regulation or other factors would decrease the accuracy. One other area of possible future application of our method is to venular trees in the GM, which have geometry similar to that of the arteriolar trees and for which it should be possible to obtain blood flow data using the streak length method.



### 3.3 References

- [1] Fry, B. C., Lee, J., Smith, N. P., & Secomb, T. W. (2012). Estimation of blood flow rates in large microvascular networks. *Microcirculation (New York, N.Y.: 1994)*, 19(6), 530-538.

# Appendices A: Figure Permission

RightsLink - Your Account

15-01-22 1:20 AM

## JOHN WILEY AND SONS LICENSE TERMS AND CONDITIONS

Jan 22, 2015

This Agreement between Amani Saleem ("You") and John Wiley and Sons ("John Wiley and Sons") consists of your order details and the terms and conditions provided by John Wiley and Sons and Copyright Clearance Center.

|                                       |  |
|---------------------------------------|--|
| License Number                        | 3511470105058  |
| License date                          | Nov 17, 2014   |
| Licensed Content Publisher            | John Wiley and Sons  |
| Licensed Content Publication          | Microcirculation   |
| Licensed Content Title                | Estimation of Blood Flow Rates in Large Microvascular Networks   |
| Licensed Content Author               | BRENDAN C. FRY, JACK LEE, NICOLAS P. SMITH, TIMOTHY W. SECOMB  |
| Licensed Content Date                 | Aug 5, 2012  |
| Pages                                 | 9  |
| Type of use                           | Dissertation/Thesis  |
| Requestor type                        | University/Academic  |
| Format                                | Print and electronic   |
| Portion                               | Figure/table   |
| Number of figures/tables              | 1  |
| Original Wiley figure/table number(s) | Figure 4. Computer-generated map of network 1. Flow directions predicted with two known boundary conditions are compared with flow directions with all boundary conditions known. Black: correct flow direction. Red: reversed flow direction. Flow Estimation in Microvessel Networks |
| Will you be translating?              | No   |
| Title of your thesis / dissertation   | ESTIMATING HEMODINAMICS IN SKELETAL MUSCLE ARTERIOLAR NETWORKS RECONSTRUCTED FROM IN VIVO DATA   |
| Expected completion date              | Jan 2015   |
| Expected size (number of pages)       | 70   |
| Billing Type                          | Invoice  |
| Billing Address                       | None<br>907-155 kent Street<br>None<br>None<br>London, ON N6A 5N7<br>Canada<br>Attn: None  |
| Total                                 | <b>0.00 CAD</b>  |
| <b>Total</b>                          |  |
| Terms and Conditions                  |  |

### TERMS AND CONDITIONS

This copyrighted material is owned by or exclusively licensed to John Wiley & Sons, Inc. or one of its group companies (each

# Curriculum Vitae

**Name:** Amani Saleem

**Post-secondary Education and Degrees:** Umm Al-Qura University (UQU)  
Faculty of Applied Science  
2004-2009 B.Sc. (Major Medical Physics)

The University of Western Ontario  
Medical Biophysics  
London, Ontario, Canada  
2012-2015 M.Sc. (Expected)

**Honours and Awards:** Scholarship for completing high education

King Abdullah Program for scholarship  
Ministry of Higher Education  
Riyadh, Saudi Arabia

**Publications:**

- 1- Baraa K. Al-Khazraji, **Amani Saleem**, Daniel Goldman, and Dwayne N. Jackson, Hemodynamic consequences of spatially-dependent sympathetic regulation in skeletal muscle arteriolar trees, Poster Presentation at the 2014 Experimental Biology, San Diego, CA, April 2014.
- 2- **Amani Saleem**, Baraa K. Al-Khazraji, Daniel Goldman, and Dwayne N. Jackson, Developing a mathematical model to predict blood flow in skeletal muscle arterioles, Poster Presentation at the 2014 London Health Research Day, London, ON, March 2014.
- 3- Baraa K. Al-Khazraji, **Amani Saleem**, Daniel Goldman, and Dwayne N. Jackson, From one generation to the next: a comprehensive account of sympathetic receptor control in branch arteriolar trees, The Journal of Physiology, submitted, February 2015.